TRANSIENT ACOUSTIC RESPONSE IN A CAR CABIN WITH LOCALIZATION OF REFLECTIONS

MASTER´S THESIS

AUTHOR: VICTOR C. LINDSTRÖM

SDU SUPERVISOR: VICENTE CUTANDA HENRIQUEZ

B&O SUPERVISORS: MARTIN BO MØLLER & PATRICK HEGATY

01/06/2013

UNIVERSITY OF SOUTHERN DENMARK.
INSTITUTE OF TECHNOLOGY AND INNOVATION.

DATOS DEL PROYECTO

Título: Transient acoustic response in car cabins with localization of reflections.
Autor: Victor Cebrian Lindström.
Programa de Postrado Oficial: Master de Ingeniería Acústica en Edificación y Medio Ambiente
Tutor: Vicente Cutanda Henriquez
Director: Vicente Cutanda Henríquez
Tribunal: Vicente Cutanda Henríquez y Peter Møller
Presidente: -
Vocal: -
Vocal Secretario: -
Fecha de Lectura: 18 Junio 2013

PREFACE.

This report is the result of my master´s thesis carried out in collaboration with the company Bang & Olufsen to put some light on the study of transient acoustic response in car cabins.

Bang and Olufsen Company, popularly known as B&O, is one of the most internationally reknown Danish manufactures on the multimedia products with a highly distinctive and exclusive range of products that combine technological excellence with emotional appeal.

I would like to thank my study fellows Manuel Vilas Alonso, Rasmus Stahlfest Holch Skov and Sebastian Kim Hjaelm Andersen for sharing their point of view on several issues along this thesis. I´m especially thankful to Henriette Bundesen and Kim Christian Bundesen for constructing the special arm-stand microphone used in the experiments. I also appreciate the contribution of Richard Cowie to the language correction of this paper.

I thank my supervisor Vicente Cutanda Henriquez for his guidelines and Martin Bo Møller for his willingness to help and brainstorming.

ABSTRACT.

Due to its small size and the restrictions on source and listener positions, the design of sound reproduction systems for car cabins is particularly cumbersome. In the present project the measurement of the impulse response between a single loudspeaker and a listener position, with special emphasis on the directional characteristics, will be examined. The propagation paths inside a car are very short, meaning that it is very difficult for the existing commercial measurement systems to resolve the different reflections arriving to the listener.

This paper propose a first approach of an algorithm based on time difference of arrival along a measurement technique aiming at finding the reflections and their direction of arrival to the listener. To this end a circular microphone array at a known position is employed, along with Maximum-Length Sequences (MLS) measurement technique. The results are processed so as to extract the directional properties, demonstrate the physical limitations that can influence or prevent this detection in practice. Measurements were carried out in a free-field environment (anechoic chamber) making use of different panels closer around the microphone array.

RESUMEN.

El diseño de sistemas de reproducción de audio para cabinas de coche es especialmente complicado debido al reducido tamaño del espacio y las restricciones de los altavoces y posiciones de escucha de los ocupantes.

En el presente proyecto, se examinan mediciones de la respuesta al impulso entre un altavoz y una posición de escucha con especial énfasis en las características direccionales. Los caminos de propagación de las ondas sonoras dentro de un coche son muy cortos, lo que hace difícil para los instrumentos de medida existentes en el mercado determinar las direcciones de llegada de las diferentes reflexiones que llegan a una posición de escucha.

Este trabajo propone una primera aproximación de un algoritmo, basado en las diferencias temporales de llegada de una onda a diferentes puntos de medida, y una particular técnica de medida de la respuesta al impulso para obtener las direcciones de llegada de reflexiones a una posición de escucha. Para ello, se emplea una matriz circular de micrófonos en una posición conocida junto con la técnica de medida MLS (Maximum Length Sequence). Los resultados obtenidos son procesados para extraer la dirección de llegada de las reflexiones acústicas y encontrar las limitaciones que influyan en la detección de dichas reflexiones. Las mediciones se llevan a cabo en un entorno de campo libre y utilizando diferentes superficies reflectantes alrededor de la matriz de micrófonos.

TABLE OF CONTENT

1 INTRODUCTION.

The stereophonic reproduction of music in car cabins is a highly complex task involving special electronic devices such as filters, delays, DSPs (digital signal processors) and FPGA (field-programmable gate array). All these systems seek the equalization of the car compartment to give a larger spatial impression and improve the quality of sound.

The reason for this is that car cabins present degraded sound quality compared to listening rooms due to the position of the loudspeakers (which is quite different from the optimal triangular stereo), narrowness of the passenger compartment, intermix of rigid and soft material limiting the direction of arrival of reflections, very short reverberation time, distribution of resonant frequencies resulting from the volume and geometry of the car compartment and so on (1). All these handicaps make conventional room acoustical parameters not directly applicable.

Some studies of the sound field in car cabins have been carried out trying offer results that could help to improve the live stereo sound.

In this way, subjective evaluation experiments like the one conducted by A.Farina and E.Ugolotti (2), based their results on volunteers point of view after listening by headphones to sound fields reconstructed by the auralization technique.

The experimental evaluation of the sound field inside a car to get reflections information is usually performed employing microphone systems having very limited capability of detecting the direction-of-arrival of wave fronts. Bellini *et al.* (3) tested a new successful high order microphone array coupled with virtual microphones methodology in a car cabin. It is based on a set of filters derived directly from a set of impulse response measurements, designed according to a least-squares principle. Results delivered higher spatial resolution compared to the resolution of low-order microphone arrays.

Systems with varying directional sensitivity can be formed by appropriately combining the signals of two or more closely spaced omni-directional microphones. An attractive feature is the possibility to vary and steer the directivity patterns later in the post processing stage. These are the so called "beamformers". Some limitations are found in classical delay-and-sum beamforming. At low frequencies the size of an array needs to be comparable to the wavelength of sound, while the spacing between the microphones used at high frequencies needs to be comparable to the wavelength at those frequencies in order to avoid spatial aliasing.

Various algorithms based on steered beamformer and subspace localization techniques have been developed like the plane-wave decomposition, eigenbeam delay and sum, eigenbeam minimum variance distortionless response, eigenbeam multiple signal classification (EB-MUSIC), and eigenbeam estimation of signal parameters via rotational invariance techniques (EB-ESPRIT) methods for localization of early reflections in room acoustic environments (4) but not many documentation was found about their tests in car cabins.

Systems based on finite difference approximation to calculate the incoming angle of a sound wave have their restrictions. At high frequencies, when the wavelength measured becomes small compared to the microphone pair separation the approximation of gradient is no longer valid. On the other hand, at low frequencies, a phase mismatch between channels will introduce a bias error (5).

This paper presents the study of a basic multi-radius microphone array of four positions an its customized algorithm for azimuth angle estimation of incoming reflections from close surfaces. The main idea of such algorithm relies on the time difference of arrival (TDOA) technique. Obtaining the impulse response at four different positions in a circular array using Maximum Length Sequence (MLS) as a exciting signal and performing correlation between them, delay time for each pair of positions is obtained. This delay time could provide the angle estimation through simple calculations. Limitations of the implementation is also analyzed through experiments and simulations.

The use of MLS signal provides clear impulse response measurements with a substantial high signal noise ratio which make it ideal as a stimulus signal. The advantages of such measurements were underline in (6). Since the same MLS signal could be exactly reproduces in different measurements, it allows to use only one microphone placed in the array microphone positions. This feature eliminates possible time delays and phase errors introduced by different microphones and the use of multi-channel systems.

Besides, since the signal measured is the impulse response of the system no restrictions are derived from gradient approximation or phase mismatch as it does in finite difference approximation.

Some assumptions and considerations taken in this study should be mentioned:

-The output of the designed system is the azimuth angle of reflections detected.

-It is not a real-time output system so computational load is not an impediment a priori.

- Far field assumed in car compartments.

- Study of different loudspeakers in car cabins can be done one by one based on the superposition principle.

- A tweeter loudspeaker is the sound source for this study.

-The system has not been tested inside a car cabin but conducted experiments pursues the reproduction of several situations that can be done inside small enclosures.

2 THEORY.

In this chapter, the theory on which the study relies is presented. TDOA sound localization technique along with MLS signal and uncertainty calculation through Monte Carlo method are the basis of the system presented in this paper.

2.1 *TIME DIFFERENCE OF ARRIVAL (TDOA) TECHNIQUE FOR SOUND SOURCE 2D LOCALIZATION.*

TDOA based systems have been widely used for more than two decades and several approached TDOA algorithm have been developed during that time (7).

Two main stages characterize TDOA technique using a microphone array with more than two microphones:

- At the first stage, TDOA is estimated for each pair of microphones performing the cross-correlation function between signals arriving at each position.

  The generalized correlation between two signals $X_1(t)$ and $X_2(t)$ is defined as (8):

$$R_{y_1 y_2}^{(g)}(\tau) = \int_{-\infty}^{\infty} \psi_{(g)}(f) G_{x_1 x_2}(f) e^{j2\pi f\tau}\ df \qquad (2.1.1)$$

  where

$$\psi_g(f) = H_1(f) H_2^*(f) \qquad (2.1.2)$$

  denotes the general frequency weighting with filters *H1(f)* and *H2(f),* and $\int_{-\infty}^{\infty} G_{x_1 x_2}(f) e^{j2\pi f\tau}\ df$ the cross power spectral density function.

  As equation (2.1.1) cannot be calculated in practice, a few finite observations of $X_1(t)$ and $X_2(t)$ are used to obtained an estimation of the output.

  The time argument at which the correlation achieves a maximum is the delay estimate Δt.

-In the second stage, classical TDOA algorithms make use of maximum likelihood or least-squares approaches to intersect the system formed by all the TDOA obtained and get the incoming angle of the signal.

First part of the TDOA technique is performed by the algorithm presented in this paper with a slight modification which will change the procedure at second stage.

For every estimate of TDOA Δt, equation (2.1.3) is applied.

$$\alpha = \sin^{-1}\frac{\mathrm{c}\cdot\Delta\mathrm{t}}{\mathrm{IMD}} \ \text{rad.} \qquad (2.1.3)$$

Where *IMD* is the inter-microphone positions distance in meters, c, obtained from equation (2.1.4), is the speed of sound in $\mathrm{m\cdot s^{-1}}$ in dry air at sea level according to (9).

$$c = \left(331.4\ \frac{m}{s}\cdot\left(\sqrt{1+\frac{\vartheta^{\circ}\mathrm{C}}{2\cdot 273.15^{\circ}\mathrm{C}}}\right)\right) \qquad (2.1.4)$$

ϑ is the temperature in degrees Celsius.

Every angle will bring along its uncertainty estimate through the Monte Carlo method.

The second stage of the algorithm differs from the general TDOA technique, as it overlaps the sectors of possible incoming reflections of all pair of microphones to get the intersection area of all of them. The angle estimation with less uncertainty that falls in that sector will be the output azimuth angle estimation of the algorithm.

2.2 *MAXIMUM LENGTH SEQUENCE SIGNAL (MLS).*

The Maximum Length Sequence signal, is a discrete sequence that switches between only two possible values (0 or 1) in an almost random way.

This sequence is generated using a digital XOR gate and a a group of *N* memory locations called *shift register* synchronously operated by a clock signal. A value is loaded in the first memory location and transferred to its neighboring cell every positive clock pulse until it reaches the output end of the register. A feedback close circuit is set taking the output of two or more cells to the XOR gate and feeding the first cell with the result. If the inputs of the XOR are adequately chosen, the resulting binary sequence will have maximum length. The longest sequence obtained before it starts repeating has a length L equal to 2^N-1. Usually, the register is initialized to all 1s. An example of a MLS generating system is illustrated in Figure 2.2.1.

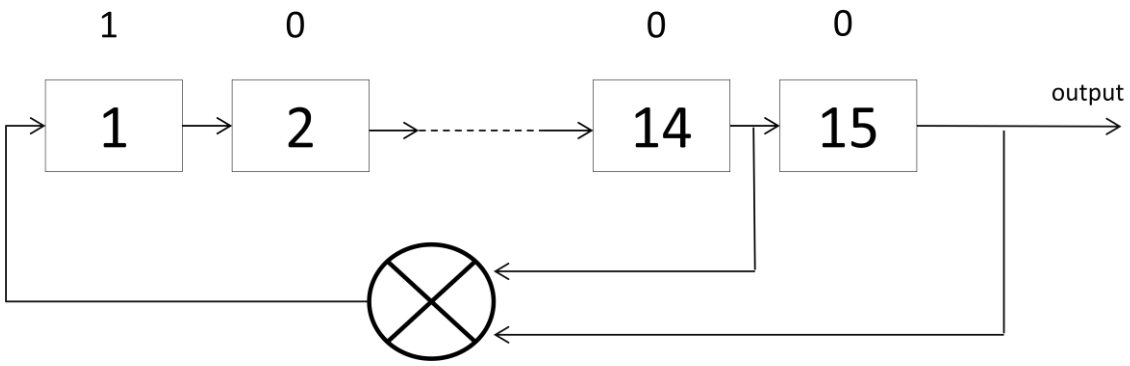

Figure 2.2.1. Diagram of a MLS generating system with a shift register of length N=15 where outputs of 14th and 15th cells are processed through a XOR gate which feeds the input of the shift register.

The binary MLS is converted to a signal as follows:

$$0 \longrightarrow +1$$

$$1 \longrightarrow -1$$

In short, the new generated signal is random but periodic with a period according to equation (2.2.1)

$$T_{MLS} = \frac{\mathrm{L}}{FC}\ s \qquad (2.2.1)$$

So that, it is also known as *pseudorandom noise.*

MLS power spectrum.

Because of the nature of this signal, there is always a *+1* value more than *-1*. Hence, the MLS signal has a DC value at the fundamental frequency f_0 and a different same value for the rest of the frequencies spaced f_0 Hz. The MLS power spectrum $\mathrm{G}(f)$ is defined by equation (2.2.2).

$$\mathrm{G}(f) = \begin{cases} \dfrac{1}{\mathrm{L}} \text{ units (DC value)}, & f = \dfrac{1}{\mathrm{T_{MLS}}} \text{ Hz} \\ \dfrac{\mathrm{L}+1}{\mathrm{L}} \approx 1 \text{ units}, & f \neq \dfrac{1}{\mathrm{T_{MLS}}} \text{ Hz} \end{cases} \qquad (2.2.2)$$

As an example, if the size of the shift register is N=15 and the clock frequency FC is 51.2 kHz. The period of the MLS signal will be:

$$T_{MLS} = \frac{\mathrm{L}}{FC} = \frac{(2^{15}-1)}{51200} = \frac{32767}{51200} = 0.63998\ s$$

The power spectrum will be:

$$G(f) = \begin{cases} \frac{1}{32767} = 3.05e^{-5} \text{ units of DC}, & f = \frac{1}{0.63998} = 1.56 \text{ Hz} \\ \frac{32767+1}{32767} = 1.00003 \text{ units}, & \text{For the rest of frequencies} \end{cases}$$

The spectral lines will be spaced 1.56 Hz and all discrete frequencies will present the same power just after a period of the MLS signal. Consequently, the power spectrum is very similar to the one of the delta impulse and the White Noise.

MLS important property.

The most important property of MLS signal is that its autocorrelation is a perfect impulse with the exception of its DC value. The normalized discrete autocorrelation ϕ at lag j for a discrete signal x_n of length L is defined in equation (2.2.3).

$$\phi_{xx}(j) = \frac{1}{L}\sum_{n=1}^{L} x_n \cdot x_{n-j} \qquad (2.2.3)$$

Indeed, for high order (big number of N) MLS signals, equation (2.2.3) delivers a maximum correlation value of 1 at zero lag and integral multiples of $L=2^N-1$ as opposed to the almost zero value of the rest of the lags. Equation (2.2.4) summarizes these results.

$$\phi_{xx}(j) = \begin{cases} 1 & j \bmod L = 0 \\ \frac{-1}{L} & \text{otherwise} \end{cases} \qquad (2.2.4)$$

An example of the autocorrelation function of a periodic MLS signal of low order N=4 is shown in Figure 2.2.2

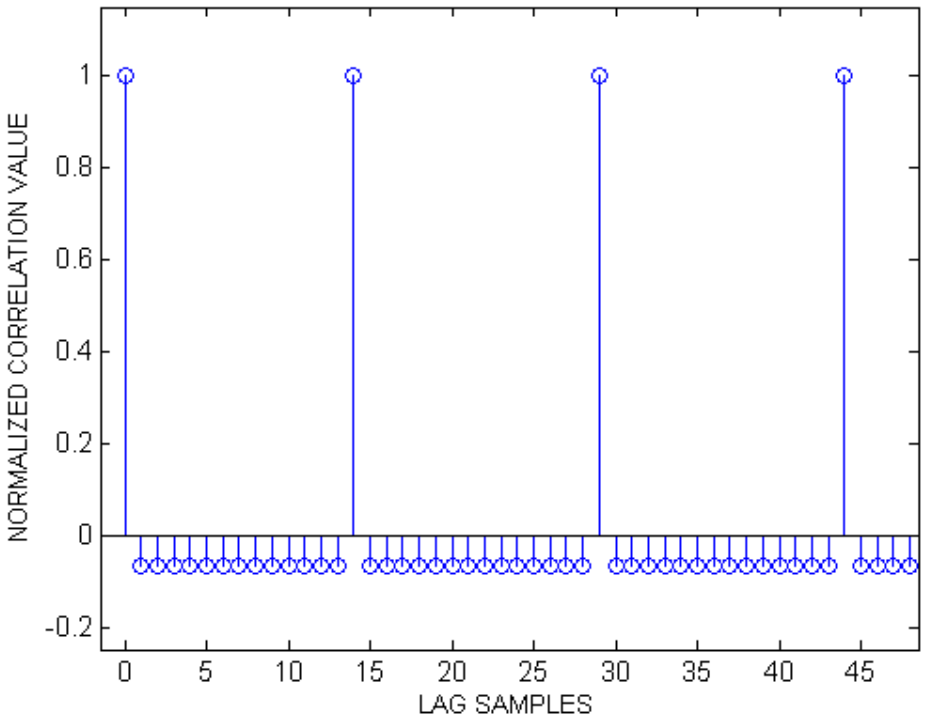

Figure 2.2.2. Normalized autocorrelation function of a periodic MLS signal of length L=15 (Order N=4). Maximum value of 1 is repeated at zero and integral multiples of L=15 lag sample.

The value of this special and important property is proved hereafter.

2.3 *IMPULSE RESPONSE MEASUREMENTS WITH MLS SIGNAL.*

One of the most beneficial procedures to obtained the impulse response of a linear time-invariant system is the one that involves the use of MLS as excitation signal.

The most important property of MLS signal is that its autocorrelation is a perfect impulse with the exception of its DC value. Therefore if the output *y[n]* of a linear time-invariant system stimulated by a MLS signal *x[n],* is defined as equation (2.3.1):

$$y[n] = h[n] \otimes x[n] \qquad (2.3.1)$$

where *h[n]* is the impulse response of the system, and $\otimes$ denotes discrete circular convolution, the cross-correlation ϕ with respect to *x[n]* on both sides of equation (2.3.1) clear the impulse response leading to equation (2.3.2)

$$h[n] = \phi_{xy} \qquad (2.3.2)$$

As MLS signal x[n] is a periodic approximate Dirac delta, the output y[n] will be periodic too with period L as well as the impulse response h[n]. Hence, L must be chosen to be sufficiently large that the transients from previous periods $h_k[n]$ of the impulse response have died down enough not to cause time-aliasing.

Benefits of measuring with MLS signal.

Several advantages are derived from the MLS features:

- MLS signal excites all frequencies equally.
- It ensures the highest possible excitation level and therefore high noise immunity.
- Output averaging can be performed between several measurements to enhance Signal Noise Ratio (SNR).
- MLS sequences are easily implemented in hardware or software, not expensive and relatively low-order feedback shift registers can generate long sequences.

2.4 *UNCERTAINTY ESTIMATION. MONTE CARLO METHOD.*

Monte Carlo method may be the most commonly applied statistical numerical method in engineering and science disciplines, used in everything from financial modeling to theoretical physics problems. The simplest form of Monte Carlo methods involves using random numbers and probability distributions to explore problems.

One of the numerous applications of Monte Carlo method for simulation is that it allows you to evaluate the uncertainty of measurement in systems which uncertainty propagation is too complex for an analytical solution.

The Monte Carlo method is characterized by getting an approximate numerical representation G, of the distribution function G_Y (ŋ*) for an output Y. The approach involves repeated sampling from the probability density function (PDFs) that characterize each input X_i, $i = 1, \ldots, N$ and the evaluation, in each case, of the model $Y = f(X)$ that relates Y and X, where $X=\{X_{1,..,}X_N\}$. The quality of these calculated results improves as the number of times the PDFs are sampled increases.

* ŋ variable describing the possible values of the output quantity Y.

The Monte Carlo method for uncertainty can provide

a) an estimate of the output quantity,

b) the standard uncertainty associated with this estimate, and

c) a coverage interval for that quantity, corresponding to a specified coverage probability.

The main stages to be followed for uncertainty evaluation using a Monte Carlo method according to (10) are:

a) **Formulation:**

1) define the measurand Y.

2) determine the input quantities $X = (X_1, \ldots, X_N)$ upon which Y depends.

3) develop a model relating Y and X.

4)Assign PDFs to the X_i.

When the X_i are independent, PDFs are assigned individually based on an analysis of a series of indications (Type A evaluation of uncertainty) or based on scientific judgement using information such as historical data, calibrations, and expert judgment (Type B evaluation of uncertainty).

b) **Propagation:** propagate the PDFs for the X_i through the model to obtain the PDF for Y.

1) select the number M of Monte Carlo trials to be made. A value of $M = 10^6$ can often be expected to deliver a 95 % coverage interval for the output quantity such that this length is correct to one or two significant decimal digits.

2) generate M vectors, by sampling from the assigned PDFs, as realizations of the (set of N) input quantities X_i.

3) for each such vector, form the corresponding model value of Y , yielding M model values.

4) sort these M model values into strictly increasing order, using the sorted model values to provide G.

c) **Summarizing:**

1) use G to form an estimate y of Y and the standard uncertainty u(y) associated with y from equation (2.4.1) and (2.4.2) respectively:

$$y = \frac{1}{n} \cdot \left(\sum_{i=1}^{M} y_i \right) \qquad (2.4.1)$$

$$u(y) = \left(\frac{1}{M-1} \cdot \sum_{i=1}^{M} (y_i - \bar{y})^2 \right)^{1/2} \qquad (2.4.2)$$

2) use G to form an appropriate coverage interval for Y , for a stipulated coverage probability p.

Let α denote any numerical value between zero and 1−p. The end points of a 100p % coverage interval for Y are $G^{-1}(\alpha)$ and $G^{-1}(p + \alpha)$.

The choice α = (1 − p)/2 gives the coverage interval defined by the (1 − p)/2- and (1 + p)/2-quantiles, providing a symmetric 100p % coverage interval.

The so called "shortest 100p % coverage" α, different from (1 − p)/2, may be more appropriate if the PDF is asymmetric. As the obtained PDF for Y is assumed to be symmetric in the experiments conducted for this report, it is left to the interested reader to get more information about asymmetric coverage in (10).

3 CIRCULAR ARRAY MEASURING SYSTEM.

Typical multi-channel circular microphone arrays for acoustic measurements are constructed with several omni-directional microphones regularly spaced mounted around a circumference or sphere. Microphone array can be used in sound source localization but gain, phase, and position errors can seriously influence the performance of localization algorithms (11). For this reason, the use of the same microphone to get the impulse response at different positions in repeated MLS measurements eliminates the gain and phase differences influence on impulse response delay time estimation between positions .

In this chapter, the features of the measuring system used to calculate the azimuth angle of reflection of sound arriving to a specific point are presented. Two main parts are differentiated:

- Hardware: set of physical components of the system.
- Software: programs and algorithms that process data.

At the same time, the number of microphone position to be selected is discussed.

3.1 *HARDWARE.*

Basic acoustic measurement instrumentation composes the set of the system. They are:

- One acoustic measurement microphone and preamplifier with low background noise.
- A standard microphone stand.
- A specially designed arm-standard holder for the microphone that allows measuring along circumferences of different radius with the microphone stand as the center of coordinates.
- A sound card of a sampling frequency 51.2 kHz to be able to sample the full audible spectrum (20 Hz - 20 kHz)
- A computer that runs the adequate software to process the impulse responses captured.
- A speaker and amplifier to reproduce the excitation MLS signal.

The hardware system specifically used in this study is shown in Table 3.1.1.

HARDWARE	COMPANY
1/2" Prepolarized free-field microphone type 4189	Brüel & Kjaer
Microphone preamplifier	Brüel & Kjaer
Stand and specially designed arm-stand and holder for microphone.	-
Symphonie Sound card. 51.2 kHz of sampling frequency	01 dB
Laptop Computer	Dell
Loudspeaker Peerless P830983 (see Annex A for specifications)	Tymphany
Power amplifier type 2706	Brüel & Kjaer
Cables for connections between equipment.	-

Table 3.1.1 The hardware system used for this study.

The main characteristic of the hardware system is the specially designed microphone arm-stand and holder for the study purposes. As shown in

Figure 3.1.1 the arm-stand is a rectangular piece of metal 14 cm long, 2 cm wide and 0.5 cm thick, with holes along its length in which the microphone can be inserted using the special microphone holder. The metal piece presents a smaller hole in one end so that it can be mounted on a standard microphone stand. The center of the holes are separated from the center of the smallest one 1.5 cm, 3.3 cm, 5.0 cm, 6.7 cm, 8.4 cm, 10 cm, and 11.8 cm, from the closest to the furthest.

As shown in Figure 3.1.2, this device allows to rotate, with different rotational radii, the microphone around the center of the microphone array located in the center of the smallest end hole of the metal plate.

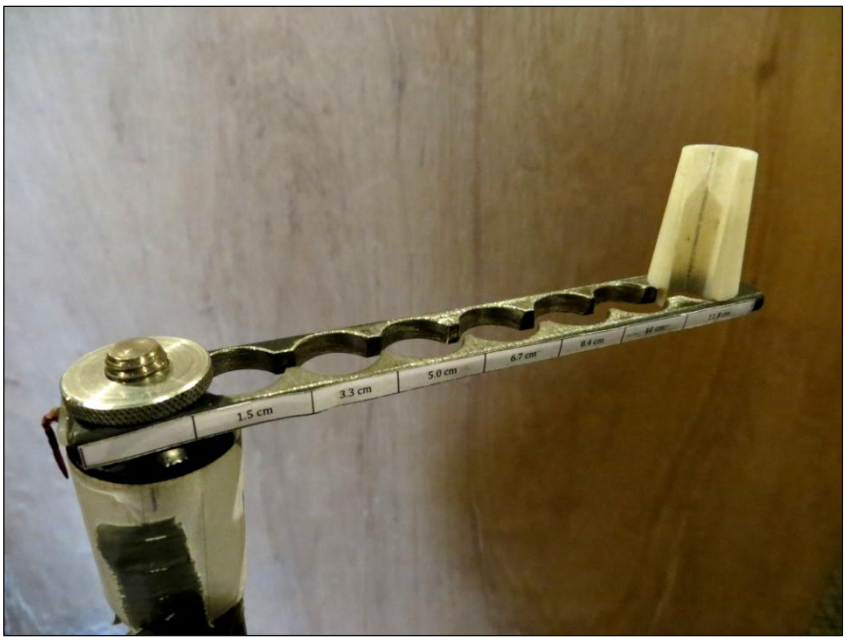

Figure 3.1.1. Microphone arm-stand and holder mounted on a standard microphone stand.

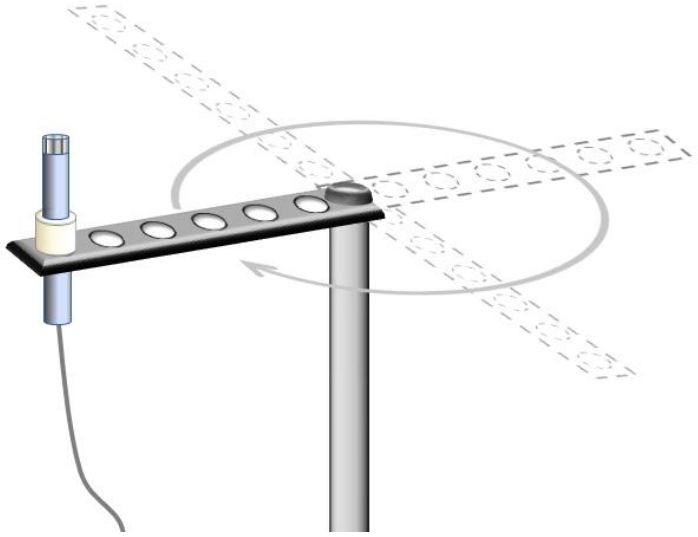

Figure 3.1.2. Single microphone array using a multi radial rotational arm-stand.

3.2 *SELECTION OF NUMBER OF MICROPHONE POSITIONS.*

The number of positions chosen for the microphone array will be critical for the results accuracy, robustness of the system and computing time.

A minimum of three equidistant positions along a circumference are required to define a two dimensional plane with equal angle resolution between pair of positions. Over this number, the angle accuracy will increase considerably and thanks to the positions redundancy the possible errors derived from a not detected reflection by one or several microphones decreases. On the other hand, The higher the number the higher the algorithm complexity and more computing time is required.

As this is a basic study of an algorithm, four positions are selected so accuracy starts to be good and the minimum redundancy of positions is taken into account. Four positions offers the possibility of still estimate a reflection angle if the algorithm fails to detect the reflection in one of the four impulse responses measured.

The array for this study was formed by four microphone positions M1, M2, M3 and M4 at angles 180º, 90º, 0º and 270º respectively forming the polar coordinates of the azimuth angle α to be measured for each reflection. An illustrative figure can be seen in Figure 3.2.1

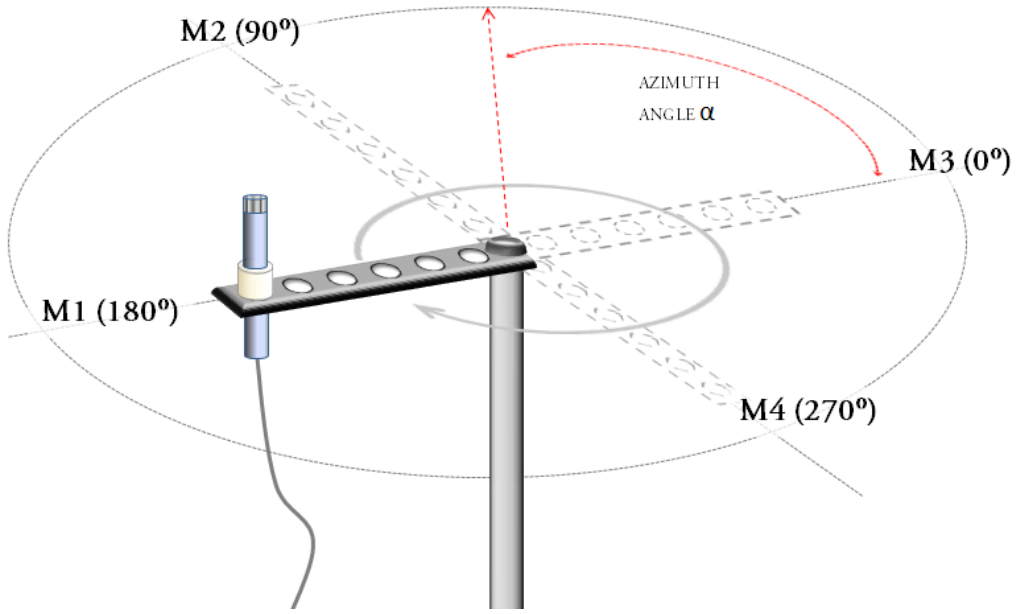

Figure 3.2.1. Microphone positions M1, M2, M3 and M4 were established as 180º, 90º, 0º and 270º for azimuth angle α polar coordinates.

3.3 *SOFTWARE.*

The general concepts of the software required for different purposes through the whole process of detecting reflections is summarized as follows:

- A software able to generate and play the MLS sequence needed for the stimulus of the whole system.
- A software that process the signal captured by the microphone to correlate it with the MLS sequence and obtain the impulse response.
- A program that process all the impulse responses obtained from the space sampled to detect reflections and elaborate an estimation of the azimuth angle of each of them.

The software used specifically in this study is schematized in Table 3.3.1

SOFTWARE	COMPANY	TASK
dBBati Version 5.1	01dB	- MLS signal generator. - Obtain impulse responses.
Algorithm_main2.m	Self made custom algorithm to be run in MATLAB	- Impulse response process for azimuth angle estimation.
MATLAB Version 7.9.0.529	The Mathworks, Inc	- Operative software for algorithm_main2.m.

Table 3.3.1. Summary of the software used in this study.

4 THE ALGORITHM.

A general overview will describe the fundamental parts of the code of the algorithm that estimates the reflection angles. Later on, their components are described in detail.

4.1 *GENERAL OVERVIEW.*

When the impulse response signals has been measured in each of the four microphone positions, they are processed in order to obtain the azimuth angle of each reflection detected. This algorithm is deployed in Matlab due to its comprehensive math and graphics functions with a powerful high-level language. In this chapter, the post processing algorithm will be explained in detail.

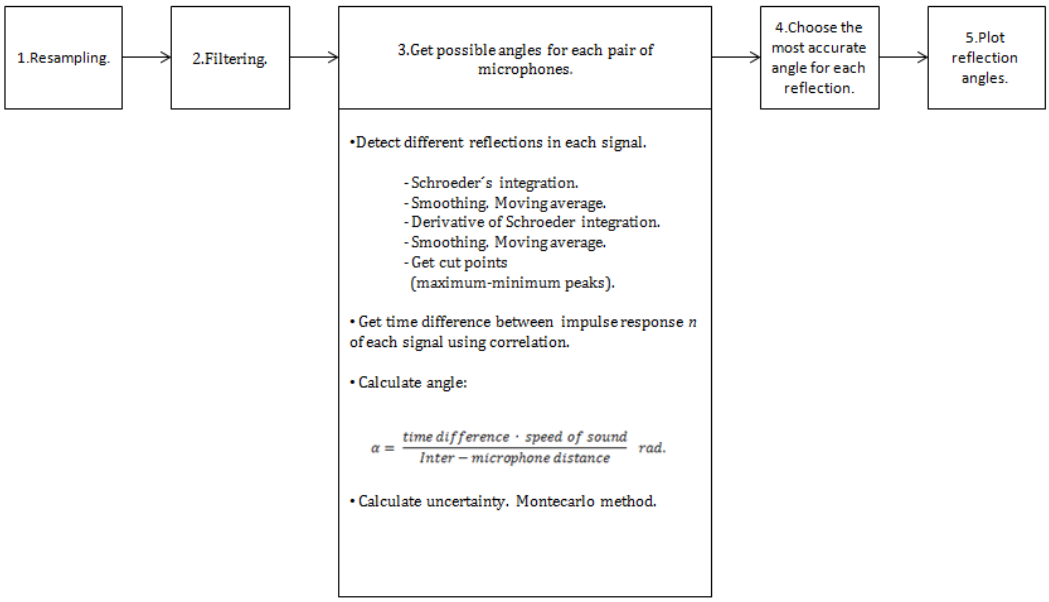

Figure 4.1.1 Algorithm general scheme.

The four impulse responses measured in positions M1, M2, M3 and M4, radial distance and the number of reflections to be calculated are the input data of the algorithm. Sampling frequency of 51.2 kHz is assumed to be used by the measuring system to convert analog impulse responses into discrete samples. Therefore, sampled signals will we broadband signals up to 20 KHz.

A schematic outline of the algorithm and its working sequence is shown in Figure 4.1.1. It follows five main stages.

A first stage of re-sampling impulse responses up to 192 kHz is performed, this is 15/4 times more than the original 51.2 kHz sampled signal . This will increase significantly the accuracy of the azimuth angle estimation and reduce the uncertainty associated to its calculation.

Stage two is an optional step. A filter can be applied to the signal to study reflections and their magnitudes in a specific frequency band. If filter is not changed in the code, the results will be associated to the whole frequency band of the input signals supplied.

The core calculations take place in stage number three. The general concept of this part is to calculate, for each reflection, the possible azimuth angles and uncertainties between every pair of microphone positions in the circular array; this is between positions M1-M3, M2-M4, M1-M2, M2-M3, M4-M3 and M1-M4. For each reflection, the most accurate angle estimated among these pairs will be chosen in stage four and plotted in stage five.

4.2 *HOW POSSIBLE AZIMUTH ANGLES ARE CALCULATED.*

As mentioned in the general overview of the algorithm, the principal operations for the possible angles estimation take place in stage three.

After stage two, given two impulse response signals of different positions, M_x and M_y, of the circular array, firstly the algorithm detects reflections in each signal. In an impulse response signal in time domain, the beginning of a new reflection is characterized by a relevant change of pressure after a dumped decay from the previous reflection. As it can be appreciated in Figure 4.2.1 four distinguishable reflection peaks of the impulse response at position M_x of the circular array are followed by their dumped decays.

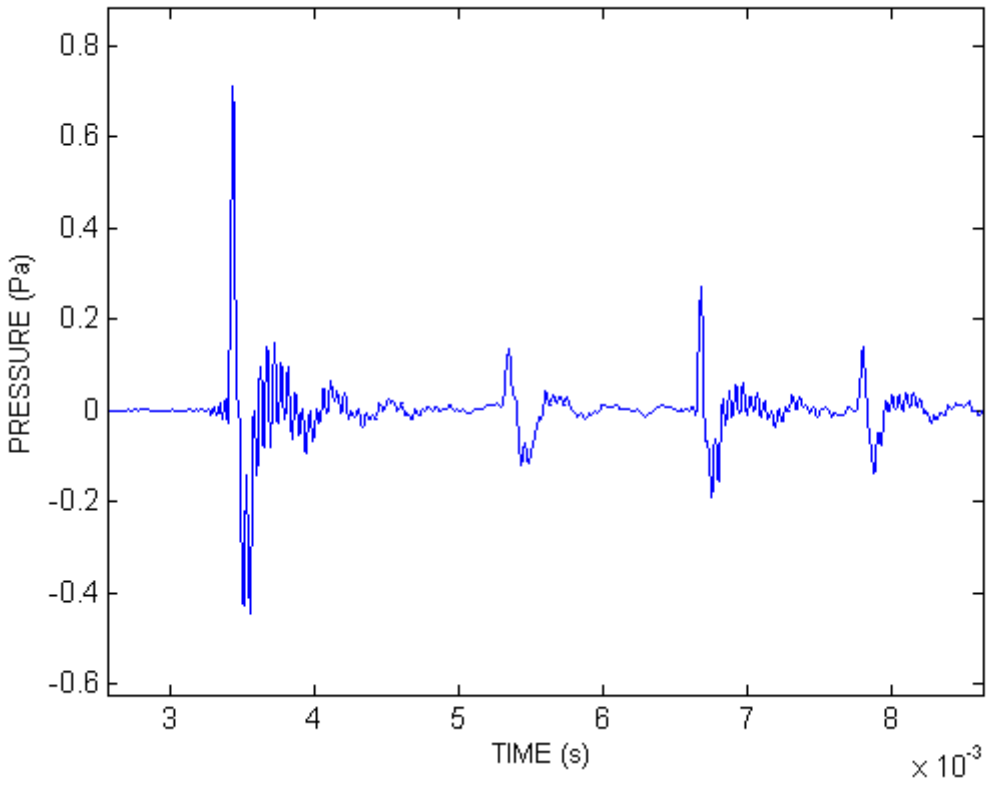

Figure 4.2.1. Impulse response signal at a M_x position

One way of finding these changes is through the calculation of Schroeder´s integration of the signal. The result signal is smoothed through a 60 points moving average filter in order to keep only the significant changes in the increasing function of time. The amount of 60 points for the moving average proved to be the optimum for most of the experiments. In Figure 4.2.2 the Schroeder´s integration curve of the impulse response plotted in Figure 4.2.1 is shown with a 60 points moving average. It is clearly observed that a significant sudden change of pressure in the signal is represented as a high slope in the Schroeder´s integration curve. More horizontal slopes mean that the reflection dumped decay almost vanishes.

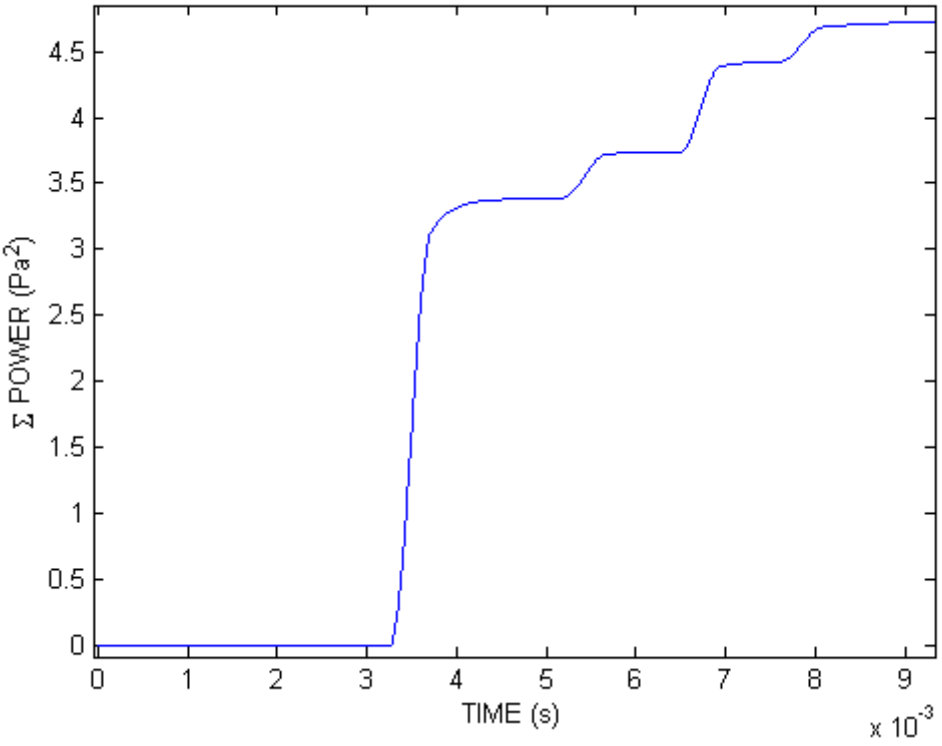

Figure 4.2.2 Representation of the smoothed Schroeder´s integration of the impulse response shown in Figure 4.2.1

The derivative of the smoothed Schroeder´s integration highlights the maximum and minimum peaks of each reflection in a clearer way as shown in Figure 4.2.3. However, the result function still requires smoothing using again a moving average filter to reduce the number of peaks and troughs to the most relevant ones. Again, a 60 points moving average proved to be the best at the experiments for optimum results.

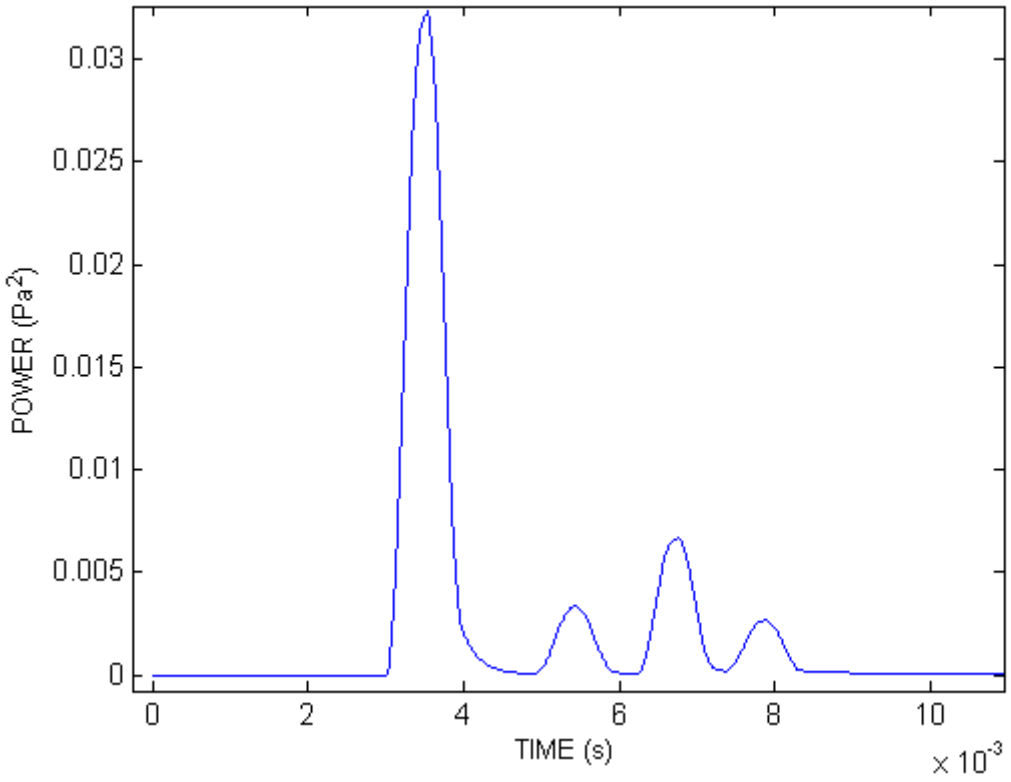

Figure 4.2.3. The derivative of Schroeder´s integration of M_x impulse responses is smoothed using a 60 points moving average to obtain only one maximum point at main peaks and one minimum at relevant valleys.

After smoothing, the beginning and ending points of reflection n^{th} are minimum peak n^{th} and $n^{th}+1$ respectively. These are the cutting points to isolate the reflection n^{th} from the whole impulse response signal. The maximum peaks will be used to offer an estimation of the sound pressure level of every reflection.

Once both signals M_x and M_y have been divided into their different reflections, correlations are performed between reflections n^{th} of each signal. A maximum value of correlation is obtained at a delay time Δt seconds from the center zero seconds of correlation. An example can be seen in Figure 4.2.4. This Δt time delay corresponds to the time it takes to the plane wave of the reflection *n* to travel from position M_x to M_y or vice versa depending on the negative or positive sign of *x* respectively.

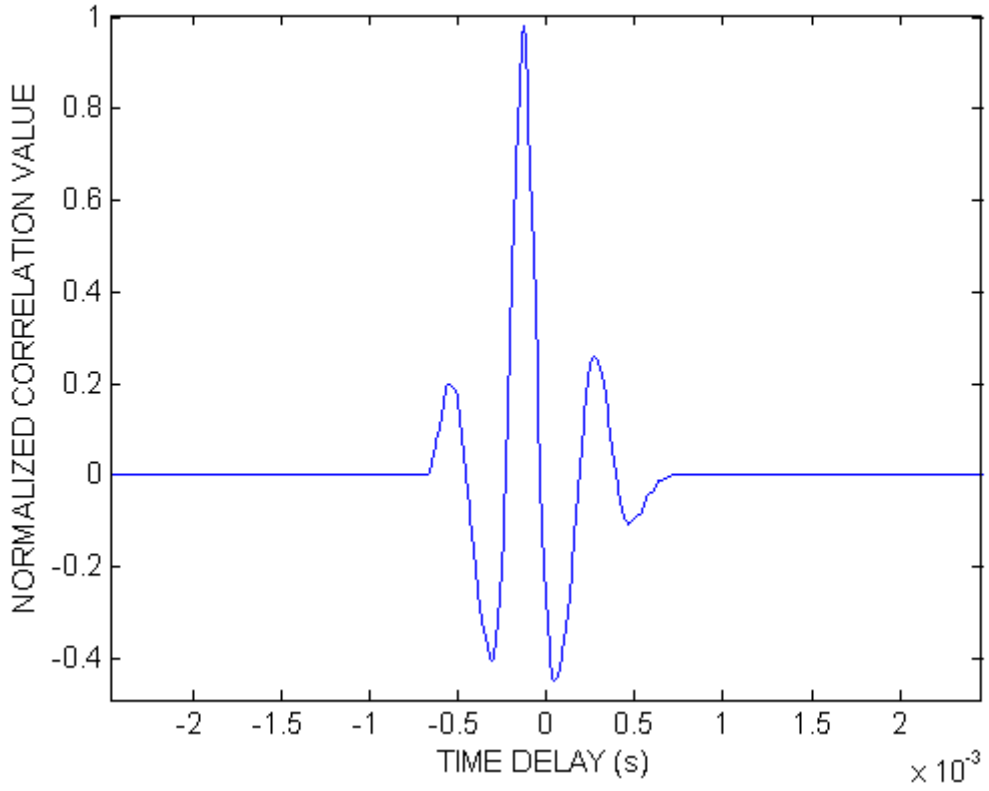

Figure 4.2.4. Correlation between division n^{th} of impulse response M_x and M_y. Maximum value of the correlation appears at the time delay between microphone positions M_x and M_y. Negative time delay means that the plane wave reached M_x before M_y. Positive time delay means that M_y was reached before M_x and time delay zero significates that both positions were reached at the same time.

The α azimuth angle estimation of the reflection n^{th} is determined by equation (2.1.3) where two results are obtained as there are always two angles between 0 and 2π which arc sine is the same. Hence, if the process to get the azimuth angle of reflections is carried out between all 6 possible combinations of the four impulse responses of the four array positions, it will give a total of 6 correlations x 2 possible angles = 12 possible azimuth angles for each reflection. At the same time, the uncertainty of the result of each angle is estimated through the Monte Carlo method (amply explained in section 4.3.)

If it turned out that the maximum correlation value is less than the minimum threshold established of 0.5, it would mean that the compared reflections were not the same and one reflection was not detected in one of the microphone positions. Although the impulse response of this microphone position will not be considered for further angle calculations, still three more impulse responses are available to calculate angles of reflections. From the moment that two microphone positions failed to detect a reflection, the algorithm cannot offer results and shows an error.

The main source code of the algorithm can be found in the CD attached under the name *Algorithm_main2.m*. The most important part of the code is found in *Reflections_Azimuth_angles2.m* function.

4.3 *UNCERTAINTY CALCULATION.*

The angle results for every reflection carries an associated uncertainty. Following the guidelines summarized in section 2.1 a MATLAB function has been developed to offer an estimated standard uncertainty for a stipulated coverage probability of 95%.

The model is built as 2.1 formulation sub-section stipulates:

1) the measurand Y is the azimuth angle **α**;

2) The input quantities $X = (X_1, \ldots, X_N)$ upon which Y depends are:

- The temperature ϑ of the room or space where the measurements take place**.** The temperature of the gas medium of propagation of sound waves influences the speed of propagation as stated in equation (2.1.4). Uncertainty in the ϑ measurement will induce an uncertainty in the measurand estimation.

- The measured discrete time delay Δt obtained from impulse response cross-correlation**.** Uncertainty in the Δt measurement will also influence in the measurand estimation uncertainty.

- The estimation of IMD† brings up an uncertainty determined by:

  - The distance r of the circular array radius measured with a caliper.

  - A deviation angle in the microphone position might be introduced when placing the microphone arm-stand in each of the four positions of the circular array. Two different situation for IMD estimation between two positions may occur:

    a) When two microphone positions are angled at 90 degrees (see Figure 4.3.1) IMD distance will be estimated from equation (4.3.1) where μ and β represent angle deviations of the microphone arm-stand of position one and two respectively.

† Inter Microphone Distance. Distance between two different microphone positions.

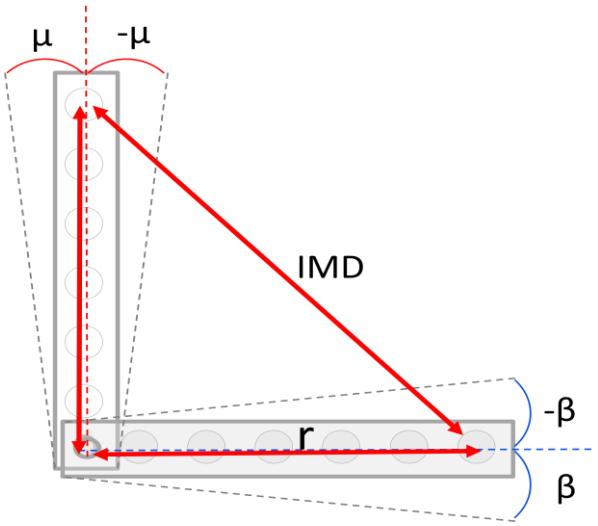

Figure 4.3.1. Two microphone positions angled 90 degrees. Position angle deviation μ and β of microphone arm-stand could vary from their desirable zero value due to the imprecision of the operator when placing the microphone.

$$IMD = \frac{\sin\left(\frac{\pi}{2} + \mu + \beta\right) \cdot r}{\sin\left(\frac{\frac{\pi}{2} + \mu + \beta}{2}\right)} \quad m \qquad (4.3.1)^{\ddagger}$$

b) When two microphone positions are angled at 180 degrees (see Figure 4.3.2 Figure 4.3.1). IMD distance will be estimated from equation (4.3.1) .

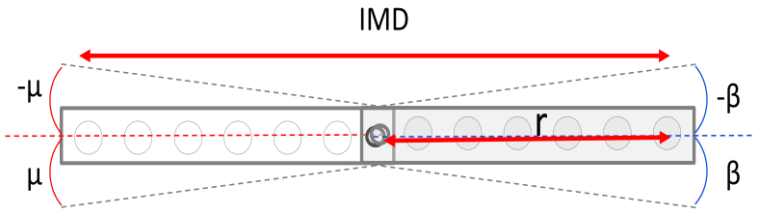

Figure 4.3.2 Positions angled 180 degrees.

$$IMD = \cos\mu \cdot r + \cos\beta \cdot r \quad m \qquad (4.3.2)$$

‡ The equation is derived from the law of sines and the fact that the positions always form an isosceles triangle.

3) Develop a model relating Y and X.

Two models are built in regard to the two IMD estimation cases.

$$\alpha = \sin^{-1}\left[\frac{\left(331.4 \cdot \left(\sqrt{1+\frac{\vartheta°C}{2\cdot 273.15°C}}\right)\right)\cdot \Delta t}{\left(\frac{\sin(90+\mu+\beta)\cdot r}{\sin\left(\frac{90+\mu+\beta}{2}\right)}\right)}\right] \text{ rad.} \qquad (4.3.3)$$

$$\alpha = \sin^{-1}\left[\frac{\left(331.4 \cdot \left(\sqrt{1+\frac{\vartheta°C}{2\cdot 273.15°C}}\right)\right)\cdot \Delta t}{\sin\mu\cdot r+\cos\beta\cdot r}\right] \text{ rad.} \qquad (4.3.4)$$

4)Assign PDFs to the X_i.

- The temperature ϑ uncertainty is due to the degrees Celsius resolution of the thermometer used for the experiments. The maximum error that could be made is 0.5°C. A rectangular PDF is assigned with a measured mean temperature ϑ°C. So that, the interval for such density function is [ϑ-0.5°C , ϑ+0.5°C]

- The PDF assigned to the measured discrete time delay Δt is rectangular of interval [Δt-1/(2·sf) *s* , Δt+1/(2·sf) *s*] where *sf* is the final sampling frequency of the signals after re-sampling. For the experiments *sf* is equal to 192 kHz

- The uncertainty of the radius r of the circular array measured with a caliper is due to the caliper *mm* resolution with a maximum error of 0.0005 m. As with previous uncertainties, a rectangular PDF is associated with an interval [r-0.0005 *m*, r+0.0005 *m*].

- Deviation angles μ and β are due to error made by the operator when placing the microphone arm-stand. Therefore, the PDF assigned is a standard Gaussian with a best estimate $x=0°\cdot\pi/180$ rad. and an estimated standard uncertainty $u(x)=3°\cdot\pi/180$ rad.

Definitions of the formulation for the Monte Carlo method are summarized in Table 4.3.1.

Y	**X_i**	**PDF**
α	ϑ ℃	Rectangular [ϑ-0.5℃ , ϑ+0.5℃]
	Δt *s*	Rectangular [Δt-1/(2·sf) *s* , Δt+1/(2·sf) *s*]
	r *m*	Rectangular [r-0.0005 *m*, r+0.0005 *m*]
	μ *rad*	Gaussian. best estimate x=0°· $\pi/180$ rad. standard uncertainty u(x)=3°· $\pi/180$ rad.
	B *rad*	Gaussian best estimate x=0°· $\pi/180$ rad. standard uncertainty u(x)=3°· $\pi/180$ rad.
MODELS I (90° angled positions)		**MODEL II (180° angled positions)**
$\alpha = \sin^{-1}\left[\frac{\left(331.4 \cdot \left(\sqrt{1+\frac{\vartheta℃}{2\cdot 273.15℃}}\right)\right)\cdot \Delta t}{\left(\frac{\sin(90+\alpha+\beta)\cdot r}{\sin\left(\frac{90+\alpha+\beta}{2}\right)}\right)}\right]$ rad.		$\alpha = \sin^{-1}\left[\frac{\left(331.4 \cdot \left(\sqrt{1+\frac{\vartheta℃}{2\cdot 273.15℃}}\right)\right)\cdot \Delta t}{\sin\alpha\cdot r+\cos\beta\cdot r}\right]$ rad.

Table 4.3.1. Summary of formulation for Monte Carlo method.

This formulation is encoded in a MATLAB function (*montecarlo_uncertainty.m*) that is included in the CD attached to this report. This function generates random numbers for each input variable from their PDFs . For each set of numbers generated, the adequate model is applied to get an output.

The process is repeated 10^6 times by the program, as recommended in *propagation* sub-section of 2.1, to obtain a large set of output values. Such results draw an approximation *G* to the distribution function of the measurand Y.

The wanted standard uncertainty is calculated from equation (2.4.2) .

The symmetry of a Gaussian PDF for *G* is assumed. For the 95% of coverage interval which indicates a factor coverage of k=2 for the calculation of the expanded uncertainty U(y) as equation (4.3.5) indicates.

$$U(y) = \mathrm{u}(y) \cdot k \qquad (4.3.5)$$

5 STUDY CASE I. THE ARRAY RADIUS INFLUENCE IN ANGLE ESTIMATION.

For this first examination of how the algorithm and the constructed array works, some experiments and simulations were conducted in order to get some information about the differences in the impulse response at different positions of the array with different radius. Some conclusions can be gathered from the results and a decision of which radius suits best for further experiments is made.

All the experiments took place in an anechoic chamber. Instrumentation and software used are summarized in Table 3.1.1 and Table 3.3.1 respectively.

All simulations were run in Odeon 10.1 Combined.

5.1 *EXPERIMENT 1.*

This is a simple experiment to study the variation of the uncertainty estimation of an incoming angle using different radii. 10 cm and 3.3 cm radius are set in the array.

The loudspeaker is facing the center of the array aligned with M1 position. A reflective panel 1.22 m high and 0.32 m wide is situated at a distance of 0.4 m parallel to the line formed by the array and the source. An illustration of the set up is presented in Figure 5.1.1

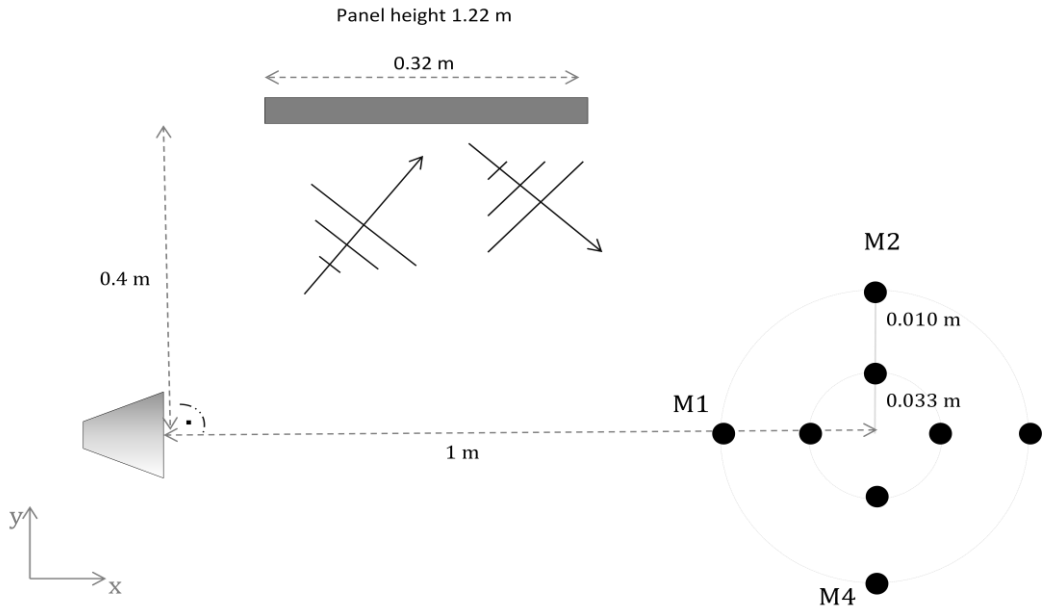

Figure 5.1.1. Set up of the experiment 1 of the study case I.

5.2 *SIMULATION 1.*

Simulation scenario was designed following the schematic illustration of Figure 5.1.1.

Set up for the simulation:

- Material assigned to the panel was 100% reflective and a 0.05 scattering coefficient.

- Omni-directional source place at the origin of coordinates at 1 meter height.

- Microphone faces the source.

5.3 *RESULTS 1.*

The results of the first experiment of the study case I for the direct sound angle estimate and the reflection are summarized in Table 5.3.1.

	Experimental angle estimation with radius 3.3 cm	Experimental angle estimation with radius 10 cm	Simulation angle estimation
Direct sound angle	$180.0^{o} \pm 4.2^{o}$	$180.5^{o} \pm 0.3^{o}$	180°
Reflection angle	$139.4^{o} \pm 2.3^{o}$	$138.6^{o} \pm 1.6^{o}$	141.34°

Table 5.3.1. Results of experiment 1 of the study case I.

Odeon plot for simulation results is shown in Figure 5.3.1.

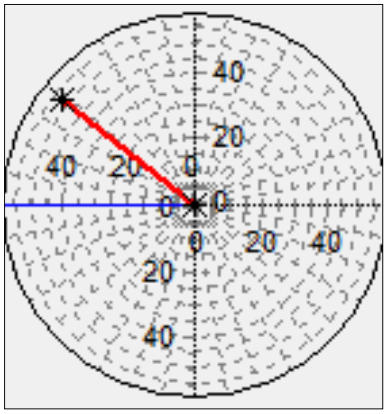

Figure 5.3.1. Simulation results with direct sound wave coming from 180 degrees azimuth angle and reflection at 141.34 degrees.

Output plots for both experimental results with radius 10 cm and 3.3 cm are shown in Figure 5.3.2 and Figure 5.3.3. respectively.

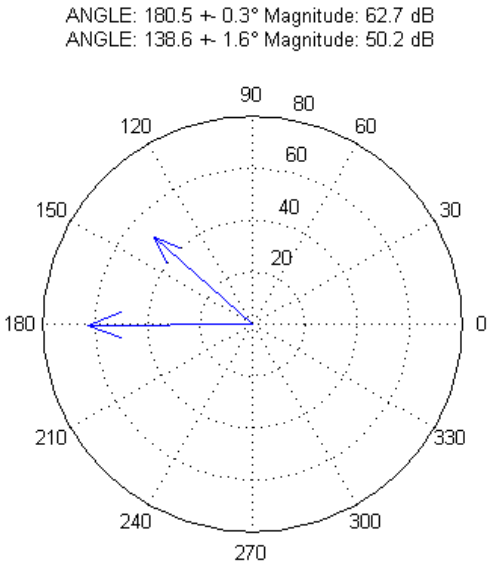

Figure 5.3.2. Output plot of the algorithm showing the estimated angles of direct sound and reflection for experiment 1 of the study case I using an array radius of 10 cm.

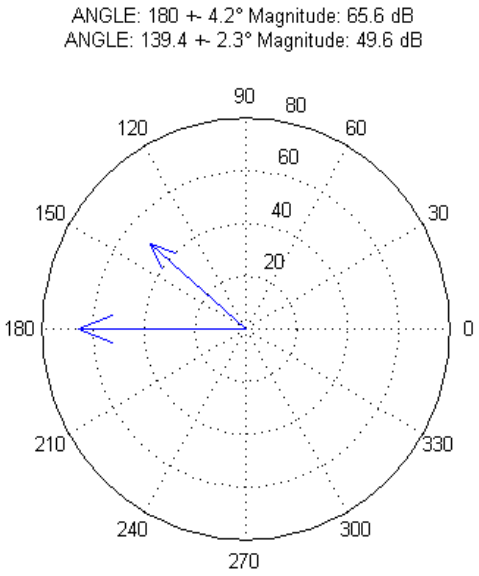

Figure 5.3.3. Output plot of the algorithm showing the estimated angles of direct sound and reflection for experiment 1 of the study case I using an array radius of 3.3 cm.

5.4 *DISCUSSION 1.*

Results for both 3.3 cm and 10 cm radius are very accurate with regard to the simulation result. Differences are found in the uncertainty associated to them. While array with radius 10 cm offers a low uncertainty of ±0.3 degrees for the direct sound and ±1.6 degrees for the reflection. The uncertainty for 3.3 cm radius array rises up to ±4.2 degrees and ±2.3 degrees respectively. Still, they can be considered acceptable.

5.5 *EXPERIMENT 2.*

The aim of this experiment is to study how much affects the diverse reflection patterns if different radii are chosen.

The experiment consists on a rectangular semi-reflecting panel situated 0.55 m from the source (tweeter speaker) on the y-axis and the microphone array center placed 1 m from the source on the x-axis as shown in Figure 5.5.1

The dimensions of the panel are 0.45 m wide and 1.20 m high. The source is a tweeter speaker facing the panel with a an angle of 45 degrees respect to the normal vector of the panel.

The source was excited with an order 15 MLS signal. A take of measurements of impulse responses are carried out at three different radius (3.3 cm, 6.7 cm and 10 cm) at M2 position of the array.

The panel was moved 5 cm parallel and towards negative x-axis each take. A total of 7 takes were performed. In the last take, the panel was slided 2 cm instead of 5 cm.

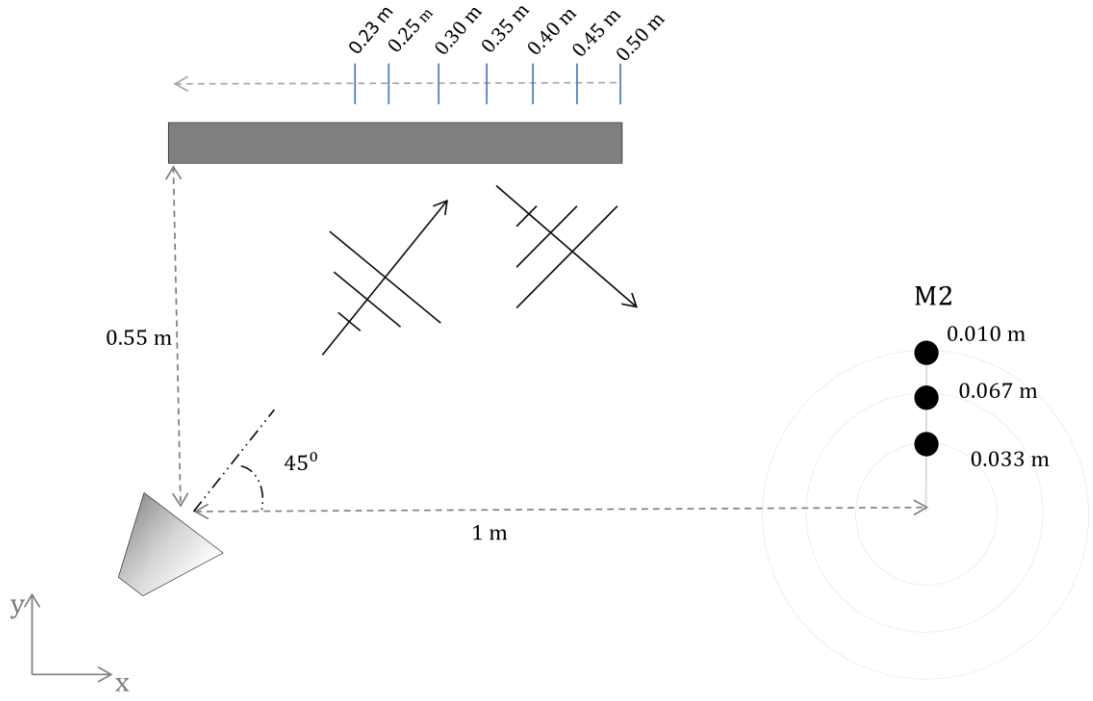

Figure 5.5.1. Schematic illustration of the experiment 2 of the study case I

In Figure 5.5.2, two pictures of the present experiment show the disposition of the elements in an anechoic chamber.

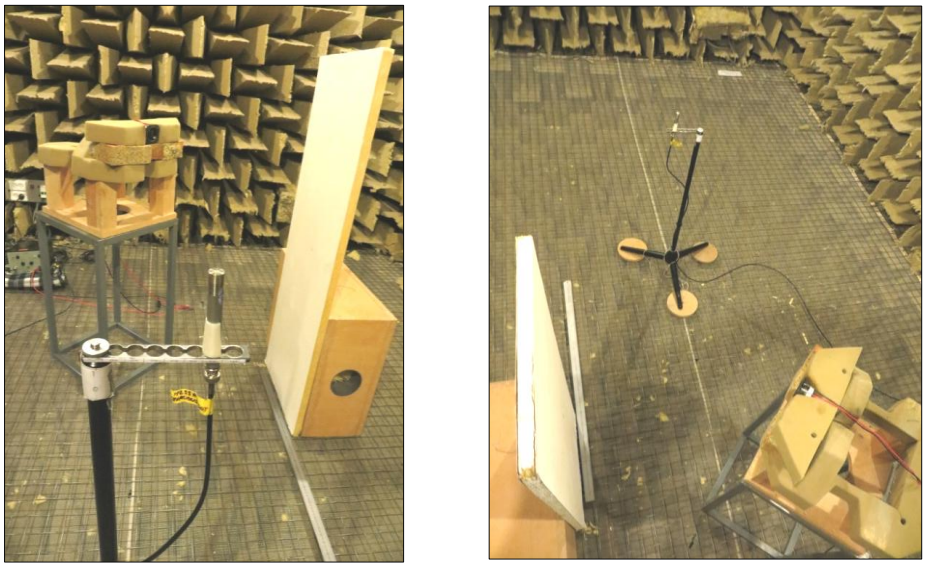

Figure 5.5.2. Two pictures of the set-up of the experiment 2 of the study case I at an anechoic chamber. Panel was pushed away from the microphone array 5 cm for each take parallel to the line formed by the source and the center of the microphone array. A ruler on the floor measured the displacements.

5.6 *SIMULATION 2.*

Five different scenarios are covered following the description of the experiments.

Due to Odeon minimum distance resolution in cm for microphone placement, the radii were adjusted. New receiver position names and radii are matched with those in the experiments in the following Table 5.6.1.

Simulation	Experiment
Position 1, radius 3 cm	Position M2, radius 3.3 cm
Position 2, radius 7 cm	Position M2, radius 6.7 cm
Position 3, radius 10 cm	Position M2, radius 10 cm
Position 4, radius 3 cm	Position M1, radius 3.3 cm
Position 5, radius 7 cm	Position M1, radius 6.7 cm
Position 6, radius 10 cm	Position M1, radius 10 cm

Table 5.6.1. Radius distance conversion from experiments to simulations.

None of the positions of the panel specified in the experiment set-up showed any reflection in the simulation. For this reason, the new distances for the right end of the panel are shown in Table 5.6.2

Simulation number	Distance
1	55 cm
2	54 cm
3	53 cm
4	52 cm
5	51 cm

Table 5.6.2. Distance on x-axis of the right end edge of the panel for each simulation.

The rest of distances and placements remain the same.

Scattering coefficient of the panel is set to minimum value of 0.05. An illustration of the simulation set-up can be seen in Figure 5.6.1

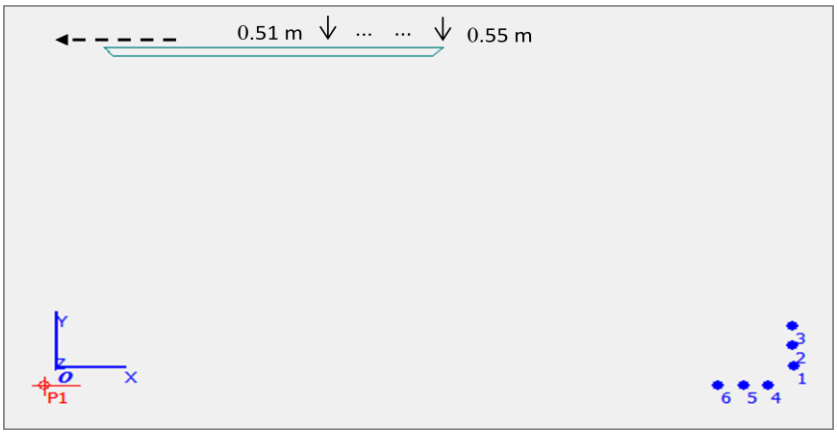

Figure 5.6.1. Odeon simulation set up with indication of 1 cm displacement on x-axis of the panel to the left starting from 0.55 m to 0.51 m (right end edge of the panel). Source is represented as P1 (in red) and 6 different position for receivers are placed on the right bottom of the figure.

5.7 *RESULTS 2.*

The outputs of the experiments are:

a) checking on the detection of the incoming reflection from the panel at M2 position with three different radius. The results are shown in Table 5.7.1.

EXPERIMENTAL RESULTS. Reflection detected.								
Position	Radius	Take 1 0.50 m	Take 2 0.45 m	Take 3 0.40 m	Take 4 0.35 m	Take 5 0.30 m	Take 6 0.25 m	Take 7 0.23 m
M2	0.100 m	✓	✓	✓	✓	x	x	x
	0.067 m	✓	✓	✓	✓	x	x	✓
	0.033 m	✓	✓	✓	✓	✓	✓	✓

Table 5.7.1. Experimental results a) of experiment 2 of study case I. Symbol ✓ means that the reflection from the panel was detected by the algorithm, on the contrary x symbol indicates no detection. X-axis Distance of the panel is shown under the number of take.

b) Get the sound pressure level (SPL) of the reflection peak of every take. The results are shown in Table 5.7.2 and plotted in Figure 5.7.1. Representation of data of Table 5.7.2.

EXPERIMENTAL RESULTS. SPL (dB) of reflection peak.								
Position	Radius	Take 1 0.50 m	Take 2 0.45 m	Take 3 0.40 m	Take 4 0.35 m	Take 5 0.30 m	Take 6 0.25 m	Take 7 0.23 m
M2	0.100 m	73.6	70.,3	67.1	62.1	60.3	57.5	57.1
	0.067 m	73.6	70.0	67.8	63.4,3	60.9	60.6	61.4
	0.033 m	74.9	71.2	68,1	64.2	62.6	63.8	63.9

Table 5.7.2. Experimental results b) of experiment 2 of study case I. SPL in dB of the reflection peak with panel placed at different distances in every take and at three different radius position.

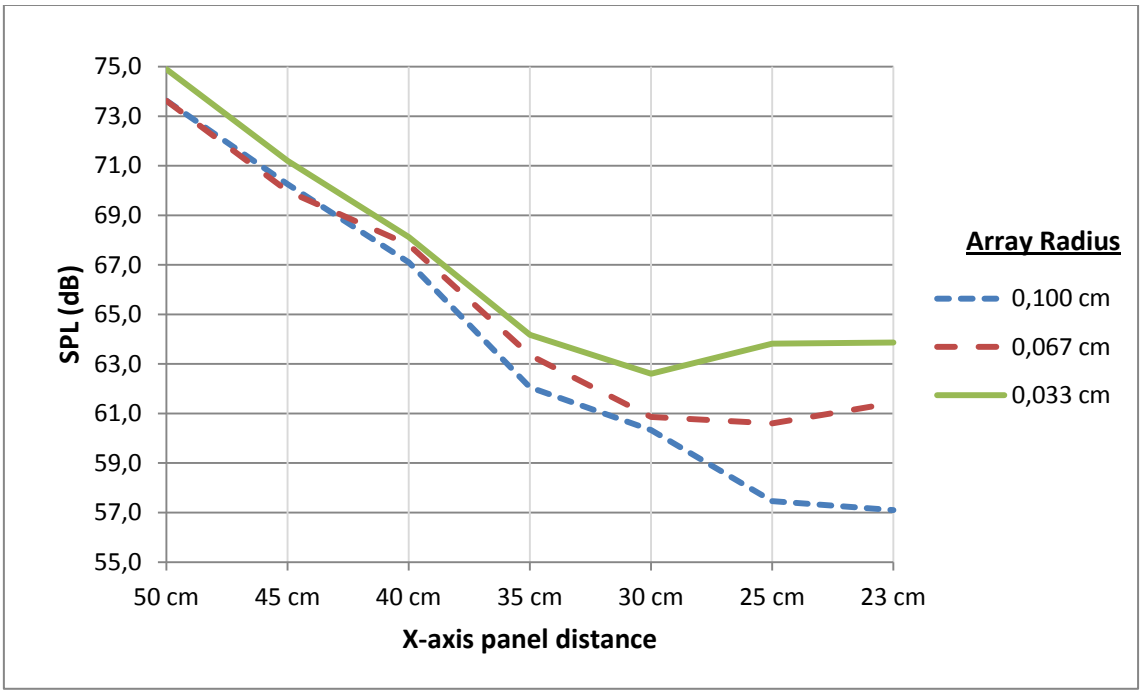

Figure 5.7.1. Representation of data of Table 5.7.2.

The simulation results of detecting reflections from the panel are set out in Table 5.7.3

SIMULATION RESULTS.						
Position	Radius	Take 1 0.55 m	Take 2 0.54 m	Take 3 0.53 m	Take 4 0.52 m	Take 5 0.51 m
M2	0.10 m	✓	x	x	x	x
	0.07 m	✓	✓	x	x	x
	0.03 m	✓	✓	✓	✓	x

Table 5.7.3. Results of simulations for the experiment 2 of the study case I. Symbol ✓ means that the reflection from the panel was detected by the algorithm, on the contrary, x symbol indicates no detection.

5.8 *DISCUSSION 2.*

Simulation results shown in Table 5.7.3 suggest that, from certain position of the panel, reflections are not detected at M2 position with 10 cm and 6.7 cm radius while using 3.3 cm radius the microphone still receives reflections from the panel. Although these results do not match reality, the main concept is visible. This is, small variations in radius distance can make a big difference in certain situations where the specular reflection area for each radius position has different material.

The experimental results seem to support this theory. As it can be seen in detected distances in Figure 5.7.1, for the specific set-up of the experiment there seems to be a limit (take5) where the reflection is only detected in M2 with radius 3.3 cm. The reflection is detected again in last take at M2 with radius 6.7 cm, and it could be due to refraction of the panel.

Experiment 3 was carried out to get more information that leads to more conclusive results.

5.9 *EXPERIMENT 3.*

Same goal as in experiment 2 is pursued.

For this experiment a particular disposition of elements were arranged to get some results that support the theory that longer radius could derived into significant differences in the impulse response between array positions.

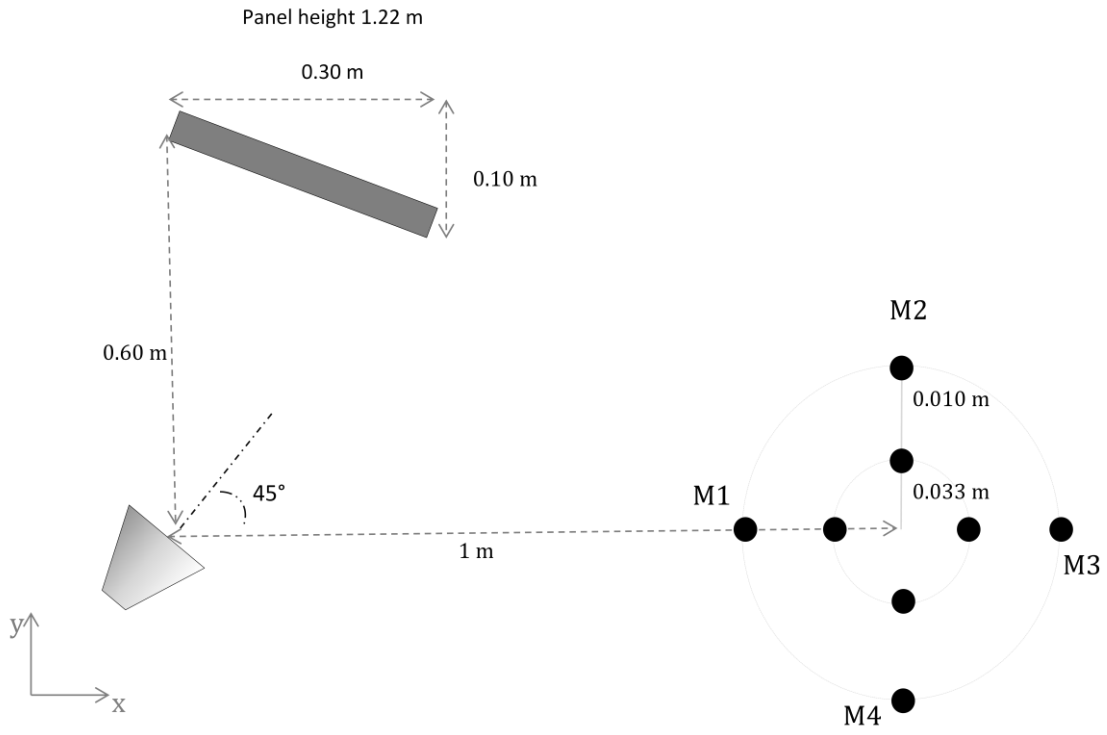

Figure 5.9.1. Set-up for experiment 3 of the study case I

The loudspeaker was arranged at 45 degrees with regard to M1 at a distance of 1 m from the array center. A reflective panel 0.32 m wide and 1.22 m long was placed at 0.60 m from the source and forming an angle of -18 degrees approximately respect to the line drawn from the center of the array and the center of the source. Both source and microphone positions were at 1 m height. The set-up of the experiment is illustrated in Figure 5.9.1.

The source was excited with an order 15 MLS signal. Impulse response is obtained with two different radius (3.3 cm and 10 cm) at all four positions of the array.

The set at the anechoic chamber can be seen in Figure 5.9.2. Picture of the set up for the experiment 3 of the study case III.

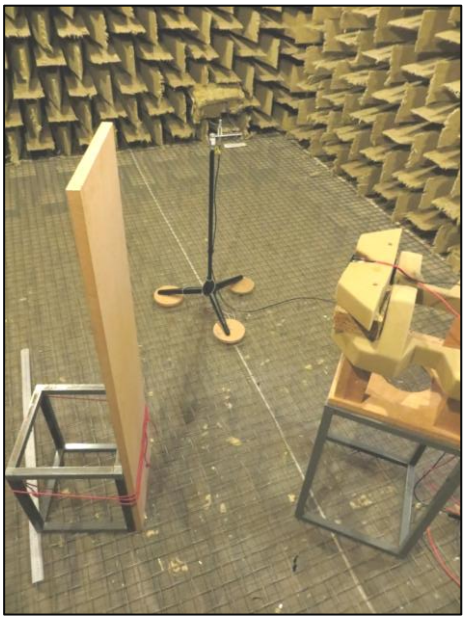

Figure 5.9.2. Picture of the set up for the experiment 3 of the study case III.

5.10 *SIMULATION 3.*

Simulation was carried out with the set-up described in Figure 5.9.1 but no reflections were detected by any receiver position.

5.11 *RESULTS 3.*

Results of the experiment number 3 are shown in Table 5.11.1.

	DIRECT SOUND ANGLE ESTIMATE	MAGNITUDE	REFLECTION ANGLE ESTIMATE	MAGNITUDE
Radius 3.3 cm	181.6° ± 0.9°	72.7 dB	152.8° ± 8.4°	29.3 dB
Radius 10 cm	Not detected	-	Not detected	-

Table 5.11.1. Result of experiment 3 of study case I.

Results of the reflections detected using 3.3 cm radius are plotted in Figure 5.11.1

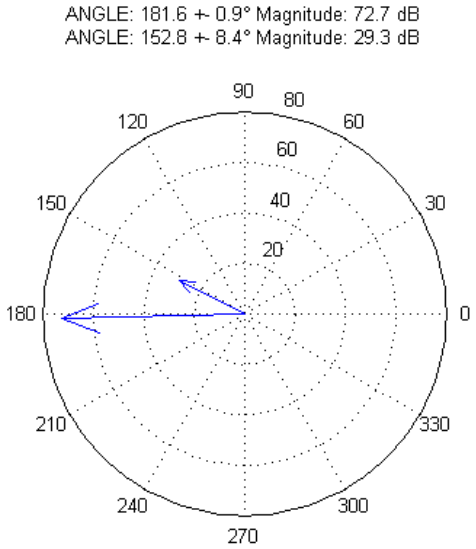

Figure 5.11.1. Output plot illustrating the estimations of direct sound (long arrow) and reflection(short arrow).

5.12 *DISCUSSION 3.*

In light of the results, the reflection seems to be detected when a shorter radius of 3.3 cm is used. The angle estimation could not be validated through simulation as it did not offer any outcome. The magnitude of 29.3 dB for the incoming reflection might indicate that the magnitude at other positions was too low to be detected.

5.13 *PARTIAL CONCLUSION OF THE STUDY CASE I.*

Two confronted situations are directly related with the size of the radius:

- The longer the radius the better the accuracy is.

- Although specular reflections and plane waves are assumed, this does not seem to fit the reality completely. At each array microphone position the reflection pattern is slightly different. The bigger the radius the greater these differences are. These variations could become more significant in small enclosures.

- A radius of 3.3 cm should probably give better performance.

6 STUDY CASE II. MINIMUM DISTANCE DETECTED BETWEEN REFLECTIONS.

In this study case, an approximation to the minimum time between reflections detected by the algorithm is discussed through experimentation.

The experiment took place in an anechoic chamber. Instrumentation and software used are summarized in Table 3.1.1 and Table 3.3.1 respectively.

The simulation was run in Odeon 10.1 Combined.

6.1 *EXPERIMENT.*

The source is facing the microphone array center at 1 m distance. Both source and receivers were at a 1 m height. As it was decided from the previous study cases, the radius of the array is 3.3 cm.

A reflecting panel was placed parallel to the line formed by the source and the center of the microphone array. Panel dimension are 1 m wide and 1.22 m high. With a high reflecting panel it is assured that the pressure level of the reflection is high enough not to merge and be mingled with the dumped decay of the direct sound impulse. The panel is 0.350 m away in the first take of the experiment and moved closer to 0.300 m, 0.250 m, and 0.200 m in the following takes.

The sound source was feed with an order 15 MLS signal to be able to excite all the audible frequency range in the system and get a maximum impulse response of 0.64 s.

In every take, four impulse responses were measured at positions M1, M2, M3 and M4 of the array.

An illustrative sketch of the set-up can be seen in Figure 6.1.1.

A picture of the experiment set in an anechoic chamber is shown in Figure 6.1.2

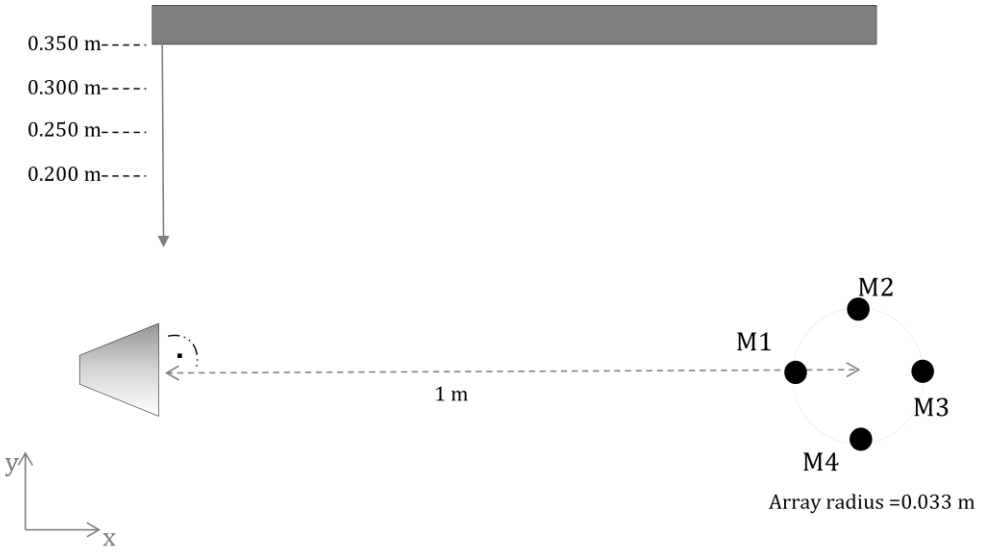

Figure 6.1.1. Set-up for the study case II. A large panel is moved 5 cm perpendicular and towards the line between source and array center every measurement.

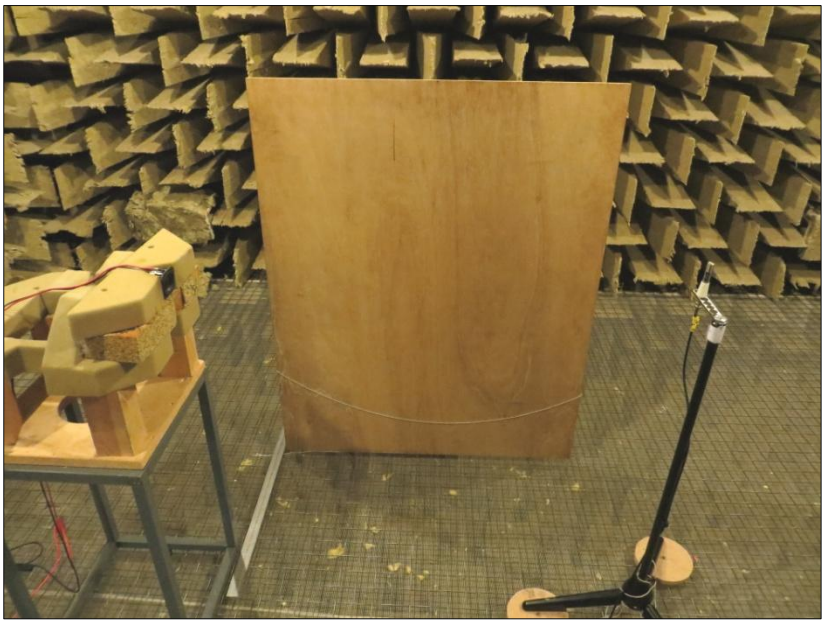

Figure 6.1.2. Set up of the study case II in an anechoic chamber.

6.2 *RESULTS.*

The results for the four takes of the experiment are shown in Table 6.2.1.

	Take 1 0.35 m	Take 2 0.30 m	Take 3 0.25 m	Take 4 0.20 m
Direct sound angle	$181.6^{o} \pm 0.9^{o}$	$181.6^{o} \pm 0.9^{o}$	$180.6^{o} \pm 4.1^{o}$	error
Reflection angle	$149.1^{o} \pm 2.4^{o}$	$152.6^{o} \pm 2.1^{o}$	157.5 ± 11.1^{o} or -157.5 ± 11.1^{o}	error
Peak to peak time distance.	$5.7292e^{-004}$ s	$4.2188e^{-004}$ s	$3.5417e^{-004}$ s	error
Algorithm detecting reflection at position	All	All	M1, M3, M4	No reflection detected at any position

Table 6.2.1. Experimental results of the study case II.

6.3 *DISCUSSION.*

Experimental results of the study case II, summarized in Table 6.2.1, offer some information about the minimum time distance between reflections to be detected.

In Take 1 and 2 no problems arose at any position to detect the reflection after the direct sound. The minimum time distance between maximum peaks of direct sound and reflection were found at position M2 in both cases.

In Take 3, were the panel was more closely situated at a distance of 0.25 m from array center and source, reflection could still be estimated but this time, the algorithm failed to detect the reflection at M2. The explanation is that the peak of the reflection was so close to the direct sound peak that it was merged in the same peak after the smoothing process of the derivative of the Schroeder´s integration signal. Due to one impulse response less to be compared with, the angle reflection was estimated with higher uncertainty of $\pm 11.1^{o}$ compared to the reflection uncertainty of $\pm 2.1^{o}$ in previous takes. Besides, there is another possible angle that fulfils the requirements when calculating from only 3 positions of the array.

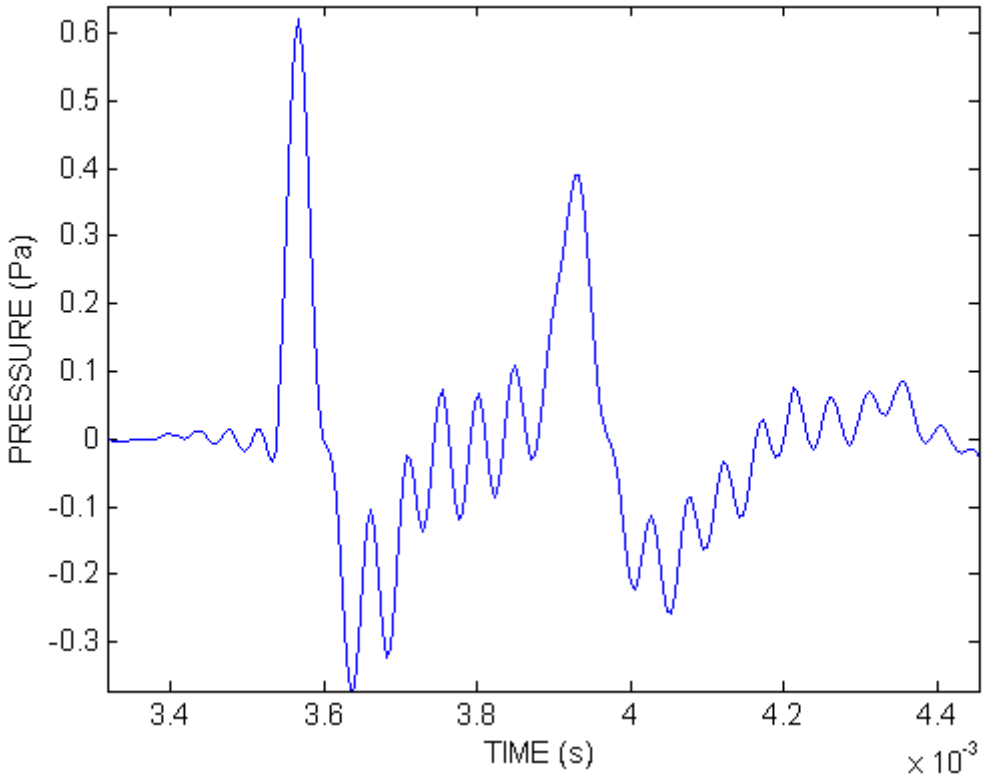

Figure 6.3.1. Impulse response at M3 in take 3 of the study case II. Direct sound peak on the left and reflection peak on the right are clearly distinguishable.

However, the main goal of this experiment was to give an approximation of the minimum time distance between reflections to be detected when reflection magnitude is high enough not to be a handicap for detection. As the algorithm did not detect any reflection at any position in take 4, the minimum time distance between two peaks of different reflections, found in M3 of take 3, is approximately estimated in $3.5417e^{-004}$ s.

A plot of the impulse response at M3 of take 3 can be found in Figure 6.3.1.

6.4 *PARTIAL CONCLUSIONS OF THE STUDY CASE II.*

From the study case II results and discussion some conclusions are derived:

- For a tweeter speaker with similar characteristics to the one used in this study, if the peak magnitude of a reflection is lower than its predecessor´s but high enough for the algorithm not to mix it with the dumped decay of the latter, the minimum distance between reflections in order to be detected is around $3.5417e^{-004}$ s.

- When one reflection is not detected for one position, in some occasions, two angle estimations are offered for one reflection in which case the result is not reliable.

7 STUDY CASE III. DETECTION OF REFLECTIONS FROM THREE CLOSE SURFACES.

The aim of this final experiment is to check how many reflections the algorithm can detect from three different panels closely placed around the microphone array.

Two experiments were conducted and simulations in Odeon were performed to validate the angle estimations offered by the system. Results are discussed leading to some partial conclusions.

The experiment took place in an anechoic chamber. Instrumentation and software used are summarized in Table 3.1.1 and Table 3.3.1 respectively

The simulation was run in Odeon 10.1 Combined.

7.1 *EXPERIMENT.*

Three panels are placed forming a square with the source as it is shown in Figure 7.1.1 along the distances between objects. The 1.20 m wide and 1.55 m long squared was chosen following the squared shape of the interior of a standard car cabin.

The array was placed at a 1 m height close to two walls as if it was the sit of a passenger in a car cabin. The 180° polar coordinate of the array was pointing at the source.

The panels were reflective with smooth surface. As they could not stand still with a perfect 90° angle respect to the floor they were slightly lean on their supports at their backs. The dimensions of the panels were as follows:

- Panel 1: 1.22 m high x 1 m long.

- Panel 2: 1 m high x 1 m long.

- Panel 3: 1.20 m high x 1 m long.

The source was placed facing the end panel (panel 2) at a 1 m height. It was supplied with an order 15 MLS signal to excite the whole audible range of frequencies in the system and get a maximum impulse response of 0.64 s.

A picture of the set arranged in an anechoic chamber is shown in Figure 7.1.2.

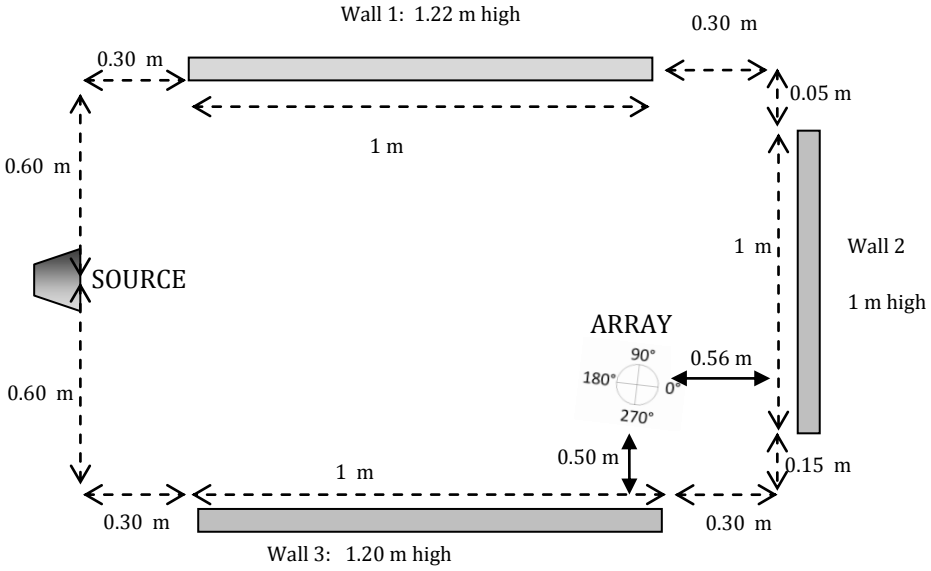

Figure 7.1.1. Set-up map of the experiments of the study case III.

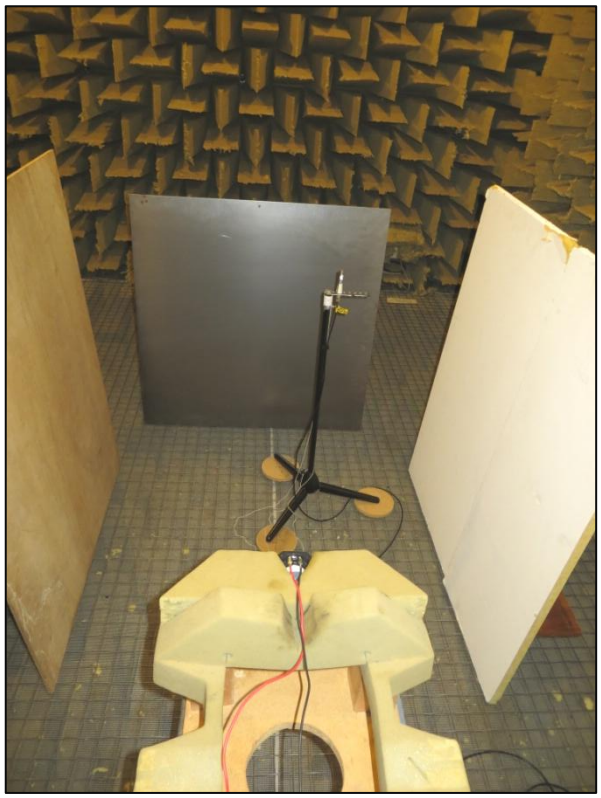

Figure 7.1.2. Set up at the anechoic chamber for the experiment of the case study III.

7.2 *SIMULATION .*

For the scenario design the dimensions of the panels and distances between objects were exactly the same as shown in Figure 7.1.1 and described at the experiment.

Some consideration were taken into account:

- Panels were also slightly angled from vertical .

- Material of panels were set as 10 % absorbent.

- Omni-directional source is assumed due to his unknown directivity pattern.

- Scattering coefficient for panels was set to the minimum value of 0.05.

- Default engineering method was selected for the simulation.

7.3 *RESULTS.*

The output data obtained from the experiment and simulation is shown in Table 7.3.1.

For the simulation angles 180° had to be added in order to compare results since azimuth angles are offered by Odeon according to the zero degrees coordinate facing the source apposite to the 180 degrees coordinate of the array pointing at the source.

REFLECTION DETECTED	SIMULATION ANGLE	EXPERIMENTAL ANGLE	EXPERIMENTAL MAGNITUDE
Direct sound	180.0°	176.9° ± 0.9°	61.4 dB
1st reflection	233.4°	233.5° ± 2.9°	37.0 dB
2nd reflection	135.9°	135.5° ± 1.4°	42.5 dB
3th reflection	12.3°	7.8° ± 1°	50.6 dB
4th reflection	340.8°	36.5° ± 2.9°	42.5 dB
5th reflection	41.5°	6.2° ± 1°	21.3 dB
6th reflection	253.2°	314.7° ± 3.9°	21.8 dB

Table 7.3.1. Simulation and experimental results. Angle estimation for direct sound and 6 reflections detected. Uncertainty and magnitude is included.

Figure 7.3.1 and Figure 7.3.2 illustrate the results from the simulation and the experiment respectively summarized in Table 7.3.1.

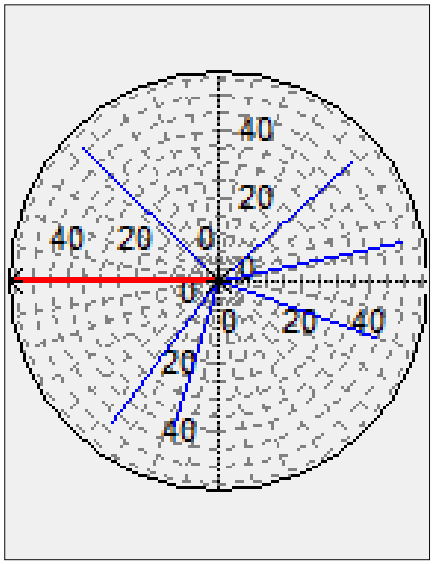

Figure 7.3.1. Azimuth angle plot obtained from simulation in Odeon 10.1 Combined. These are the angle results shown in Table 7.3.1.

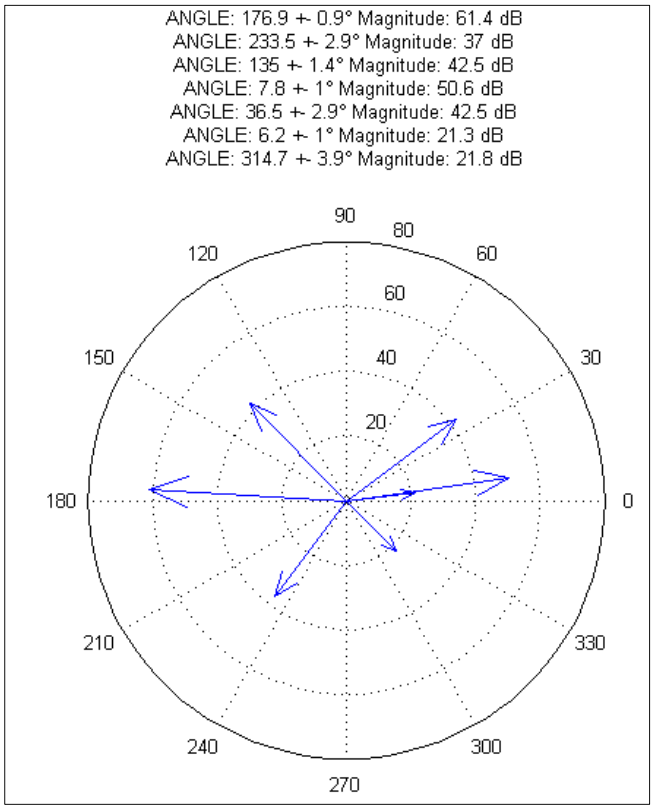

Figure 7.3.2. Experimental results representation. It is the output plot of the algorithm. Direct sound and 6 reflections incoming angle estimations are drawn in a polar coordinate plot. The length of the arrows describes the maximum SPL magnitude of the reflection in dB. Scale of magnitude is labeled on each concentric circumference. Angle labels are placed around and outside the largest circumference. Data is printed at the top for clearer interpretation of the plot.

7.4 *DISCUSSION.*

If simulation plot in Figure 7.3.1 is compared to experimental results plot in Figure 7.3.2, at least five reflections seem to be similar, one of those is the direct sound at approximately 180 degrees. From Table 7.3.1 it can be said that the direct sound and the first three reflections got from the experiment match simulation results while the rest do not if they are compared in the same order.

However, the 4th reflection of the experimental results and 5th reflection from simulation are very close. It could mean that the algorithm did not detect the 4th reflection pointed by the simulation and jumped straight to detect the reflection number five of the simulated model.

The 5th and 6th reflection detected at the experiment do not match any possible angle showed by the simulation. It does not mean that they do not exist as they can be due to different reflection patterns from specular reflection. On the other hand, they could be done from errors caused by the smoothing process at the end of the impulse response.

7.5 *PARTIAL CONCLUSIONS OF THE STUDY CASE III.*

The algorithm delivered some satisfactory results with at least 3 reflections and the direct sound azimuth angle estimation with low uncertainty between ±1 and ±3 degrees.

However, more experiments should be carried out in more complex environment with more surfaces in order to push the algorithm to its limits and see if it can cope with other real scenarios.

8 FINAL CONCLUSIONS.

In this report a different approach to TDOA technique for reflection localization was presented. Its performance and constraints wanted to be study for its possible development and application in small enclosures as car cabins.

Based on the results of this report and the interaction with the algorithm during its implementation some conclusions are presented.

Building up an algorithm to detect reflections is not an easy task specially when small enclosures are involved.

On one hand, only with four array positions the algorithm delivered quite accurate results with low uncertainty for simple environment experiments. It did not required high computational load and it could even detect some reflections mingled with the dumped decay of the direct sound impulse.

Small radii microphone arrays are suggested due to significant differences on impulse responses at different positions of the array. Accuracy can be increase adding more measuring points in the array.

On the other hand, reflections are dismissed when their magnitude is low enough to be compared to the dumped decay peaks of the previous reflection or direct sound impulse. In order to be detected, impulses of reflections should be spaced at least $3.5417e^{-004}$ s with enough magnitude.

During testing, It turned out that some values for the moving average (smoothing) of signals did mask some reflections peaks and detected others while different values uncover the firsts and dismissed the latter and sometimes even giving false outcome. For that reason, a value for the moving average was set to be the optimum. However, this issue proves that this first stage of the algorithm is not reliable enough.

Although some alternative tests results with band pass filtered impulse responses have not been included in this paper, it should be mention that the results were not satisfactory.

Some future steps to improve the performance of the system are mentioned in the following chapter.

9 FUTURE STEPS.

As a first approach, the algorithm showed some interesting results but some features can be improved.

- Adding more microphone positions, accuracy will increase and possible errors can be reduced thank to a higher redundancy of impulse responses.

- The second stage of the algorithm, where intersection of sectors for angle selection is process, can be enhanced using the least squared estimation.

- Other possible treatment of the impulse responses to obtained estimations of reflections could be based on sum and delay beamforming. This could be done adding an appropriate delay to the impulses for a specific angle to steer the beamformer and read the signal over time synchronously in all impulses. Sound pressure levels are summed to find an incoming reflection angle when a peak is detected.

- Further developments of the array could consider the elevation angle estimation for a complete 3D spatial sampling.

10 REFERENCES.

1. *Sound field control in a car compartment.* **Chono, Takeshi, Yamato, Toshitaka and Ito, Tatsuo.** s.l. : FUJITSU TEN Tech, 1988.

2. *Subjective evaluation of the sound quality in cars by the auralisation technique.* **Farina, Angelo and Ugolotti, Emanuele.** Parma : s.n., 1997. 4th International Conference and Exhibition Comfort in the automotive industry.

3. *Experimental analysis of spatial properties of the sound field inside a car employing a spherical microphone array.* **Binelli, Marco, et al.** London, U.K. : s.n., 2011. 130th AES Convention.

4. *Localization of distinct reflections in rooms using spherical microphone array eigenbeam processing.* **Sun, Haohai, et al.** 4, s.l. : Acoustical Society of America, April 2012, J. Acoust. Soc. Am., Vol. 131.

5. **Brüel & Kjaer.** *Sound intensity booklet.* 1993.

6. **Blanco Galindo, Miguel.** *Measurement techniques for microphone array calibration.* Acoustic group. Institute of Technology and Innovation, University of Southern Denmark. Odense, Denmark : s.n.

7. **Rui, Yong and Florencio, Dinei.** *New direct approaches to robust sound source localization.* Redmond, WA : Microsoft Research.

8. *The generalized correlation method for estimation of time delay.* **Knapp, Charles H. and Carter, G.Clifford.** 4, August 1976, IEEE Transactions on acoustics, speech and signal processing., Vols. ASSP-24.

9. *Environmental Effects on the Speed of Sound.* **Bohn, Dennis A.** No. 4, Rane Corporation, Mukilteo, WA 98275 USA : J. Audio Eng. Soc., 1988 April, Vol. Vol. 36 .

10. **Joint Committee for Guides in Metrology, Working Group 1.** *Evaluation of measurement data - suplement 1 to the "Guide to the expression of uncertainty in measurements" - Propagation of distributions using a Monte Carlo method.* s.l. : JCGM, 2008.

11. *A new calibration method for microphone array with gain, phase and position errors.* **Xiao, Hua, Shao, Huai-Zong and Peng, Qi-Cong.** 3, September 2007, Journal of electronic science and technology of China, Vol. 5.

12. **H. Johnson, Don and E.Dudgeon, Dan.** *Array signal processing. Concepts and technics.* s.l. : Prentice hall.

13. *Applications of a 3D Microphone Array.* **Merimaa, Juha.** Munich, Germany : Audio Engineering Society, 2002. Convention paper 5501.

ANNEX A. SOURCE SPECIFICATIONS.

TYMPHANY

Transducer Specification Sheet

Model Number: PLS-P830983
Product Line: Peerless Gold

Revision: Rev 1_0
Date: 9-Sep-09

Peerless

Product Description:

This 2 inch 4 ohm member of the PLS family sets a high standard, for compact full range drivers intended for applications such as television soundbars and compact music systems. Design features in this family include a damped plastic basket with venting under the spider to aid cooling of the motor, a neodymium magnet motor with copper cap to lower coil inductance, providing low distortion at low frequencies and extended high frequency response. A black anodized aluminium cone is employed on the driver, along with a black anodized aluminium dust cap coupled directly to the voice coil. Additionally, the cones come equipped with special-designed large roll rubber surrounds, which allow for a dynamic linear response to high excursion input signals.

Specifications:

DC Resistance	R_{evc}	Ω	3.6	5.0%	Energy Bandwidth Product	EBP	$(1/Q_{es})\cdot f_s$	217
Minimum Impedance	Z_{min}	Ω	4.0	7.5%	Moving Mass	M_{ms}	g	1.64
Voice Coil Inductance	L_e	mH	0.03		Suspension Compliance	C_{ms}	um/N	502.3
Resonant Frequency	f_s	Hz	176	15.0%	Effective Cone Diameter	D	cm	4.4
Mechanical Q Factor	Q_{ms}	-	5.6		Effective Piston Area	S_D	cm^2	15.2
Electrical Q Factor	Q_{es}	-	0.81		Equivalent Volume	V_{as}	L	0.16
Total Q Factor	Q_{ts}	-	0.71		Motor Force Factor	BL	T-m	2.83
Ratio f_s / Q_{ts}	F	f_s / Q_{ts}	248		Motor Efficiency Factor	β	$(T\cdot m^2)/\Omega$	2.22
Half Space Sensitivity @ 2.83V	dB@2.83V/1m	dB	85.0	+/-1.0 [1]	Voice Coil Former Material	VC_{fm}	-	Aluminum
Sensitivity @ 1W/1m	1W/1m	dB	82.2	+/-1.0 [1]	Voice Coil Inner Diameter	VC_d	mm	25.7
					Gap Height	Gh	mm	3.0
Rated Noise Power (IEC 2685 18.1)	P	W	7		Maximum Linear Excursion	X_{max}	mm	1.65
Test Spectrum Bandwidth	150Hz - 20kHz		12 dB/Oct		Ferrofluid Type	FF		N/A
					Transducer Size	-	Inch	2
					Transducer Mass	-	kg	0.14

1 - Piston Band Sensitivity Tolerance

Frequency and Impedance Response:

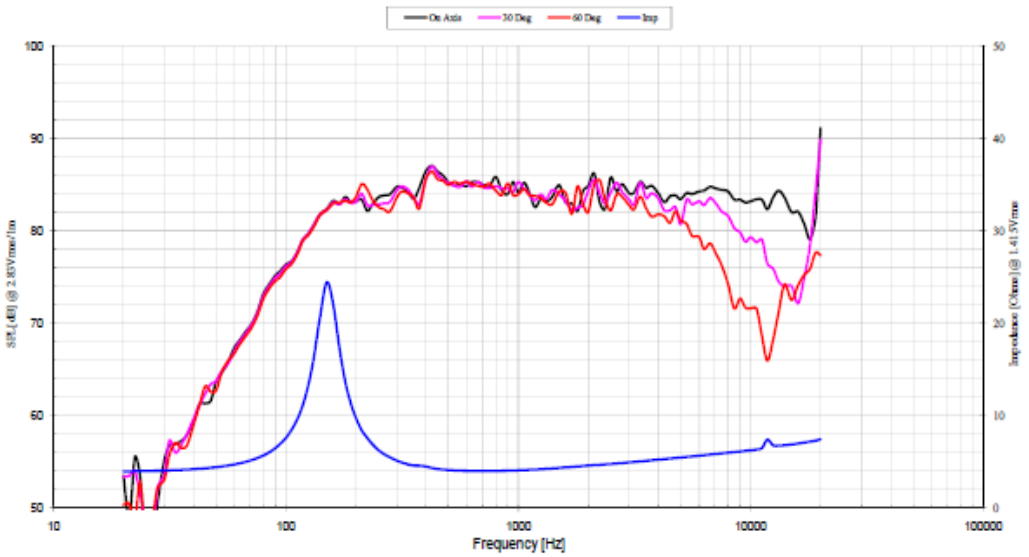

Tymphany HK Ltd
Address : Room 1307-8 Dominion Centre, 43-59 Queen's Rd East, Wanchai, Hong Kong
E-mail: sales@tymphany.com